

Contents lists available at ScienceDirect

Tectonophysics

journal homepage: www.elsevier.com/locate/tecto



Cenozoic multi-phase deformation in the Qilian Shan and out-of-sequence development of the northern Tibetan Plateau



Bing Li^{a,b,c}, Andrew V. Zuza^c, Xuanhua Chen^{a,b,*}, Daogong Hu^d, Zhaogang Shao^{a,b}, Bangshen Qi^d, Zeng-zhen Wang^{a,b}, Drew A. Levy^c, Xiaosong Xiong^{a,b}

- ^a Chinese Academy of Geological Sciences, Beijing 100037, China
- ^b SinoProbe Center, Chinese Academy of Geological Sciences and China Geological Survey, Beijing 100037, China
- c Nevada Bureau of Mines and Geology, University of Nevada, Reno, Nevada 89557, USA
- ^d Institute of Geomechanics, Chinese Academy of Geological Sciences, Beijing 100081, China

ARTICLE INFO

Keywords: Cenozoic Multi-phase Out-of-sequence development Qilian Shan Northern Tibetan Plateau

ABSTRACT

Uplift of the Tibetan Plateau and the distribution of deformation across it are the result of India-Asia collision, which bring an opportunity of understanding intracontinental tectonics in the context of continent-continent collision. The Tibetan Plateau is bound on the northern margin by the Qilian Shan thrust belt and the strike-slip Haiyuan fault. These Cenozoic fault systems play a critical role in accommodating continental convergence, yet the initiation age, deformation sequence and mechanisms of deformation are debated. In this study, integrated geologic mapping, field observations, and apatite fission track thermochronology were conducted to constrain the initiation ages of the localized thrust faults and the exhumation history of the central and northern Qilian Shan, northern Tibet. Our analyses reveal the central and northern Qilian Shan underwent rapid cooling during the Cretaceous as a result of a far-field tectonic event. In the Eocene-Oligocene, a period of thrust-related cooling occurred along the Shule Nan Shan, Tuolai Nan Shan and Tuolai Shan faults. Reactivation of the proximal thrust faults and initiation of the western segment of the Haiyuan fault occurred at ca. 16 Ma and drove final accelerated Miocene cooling and denudation to the surface. We argue that the Qilian Shan thrust belt has persisted as the stationary and internally deformed northern boundary of the Himalayan-Tibetan orogen since the early Cenozoic, involved overprinting out-of-sequence development starting by Eocene related to initiation of India-Asia collision, and the basins and ranges across the northern Tibetan Plateau have since experienced multi-phase of growth.

1. Introduction

The most significant consequence of India-Asia continental collision is the formation of Himalayan-Tibetan orogen and related Tibetan Plateau (Yin and Harrison, 2000; Yin, 2006, 2010; Royden et al., 2008; Wang et al., 2014) (Fig. 1A). Despite decades of research focused on the evolution of the Tibetan Plateau, the spatial-temporal distribution, timing and mechanism of upward and outward growth, and its impact on global climate are still debated (Raymo and Ruddiman, 1992; Meyer et al., 1998; Clark, 2012; Hough et al., 2011; Molnar et al., 1993, 2010; Royden et al., 2008; Tapponnier et al., 2001; Wang et al., 2008, 2014; Lin et al., 2016). Addressing the questions of how and when the Tibetan Plateau reached its modern elevation and extent can help us understand processes of continental deformation and plateau construction (Burchfiel et al., 1991; Tapponnier et al., 2001; Wang et al., 2008; Yin,

2010; Clark, 2012; Wang et al., 2016a, 2016b; Zuza et al., 2016a).

The northeastern margin of the Tibet Plateau is defined by the 350-km-wide, 1300-km-long active Qilian Shan thrust belt (e.g., Meyer et al., 1998; Yin and Harrison, 2000; Zuza et al., 2018) (Fig. 1). The Cenozoic tectonic evolution of these fault systems is critical to understanding the kinematics and mechanisms of plateau development. At the northeastern plateau margin, crustal thickening and active shortening are distributed across a wide region extending from the left-slip Kunlun fault in the south to the Hexi Corridor. The Cenozoic Qilian Shan thrust belt is commonly recognized as the northeastward growth front of the Tibetan Plateau (Tapponnier et al., 2001; Zheng et al., 2017), but precise age estimates for the initiation of its structures, and the style and mechanisms of range growth are poorly resolved. Various data sets suggest the Qilian Shan thrust belt experienced Eocene shortening shortly after India-Asia plates collision (e.g., Dupont-Nivet)

^{*}Corresponding author at: Chinese Academy of Geological Sciences, Beijing 100037, China. E-mail address: xhchen@cags.ac.cn (X. Chen).

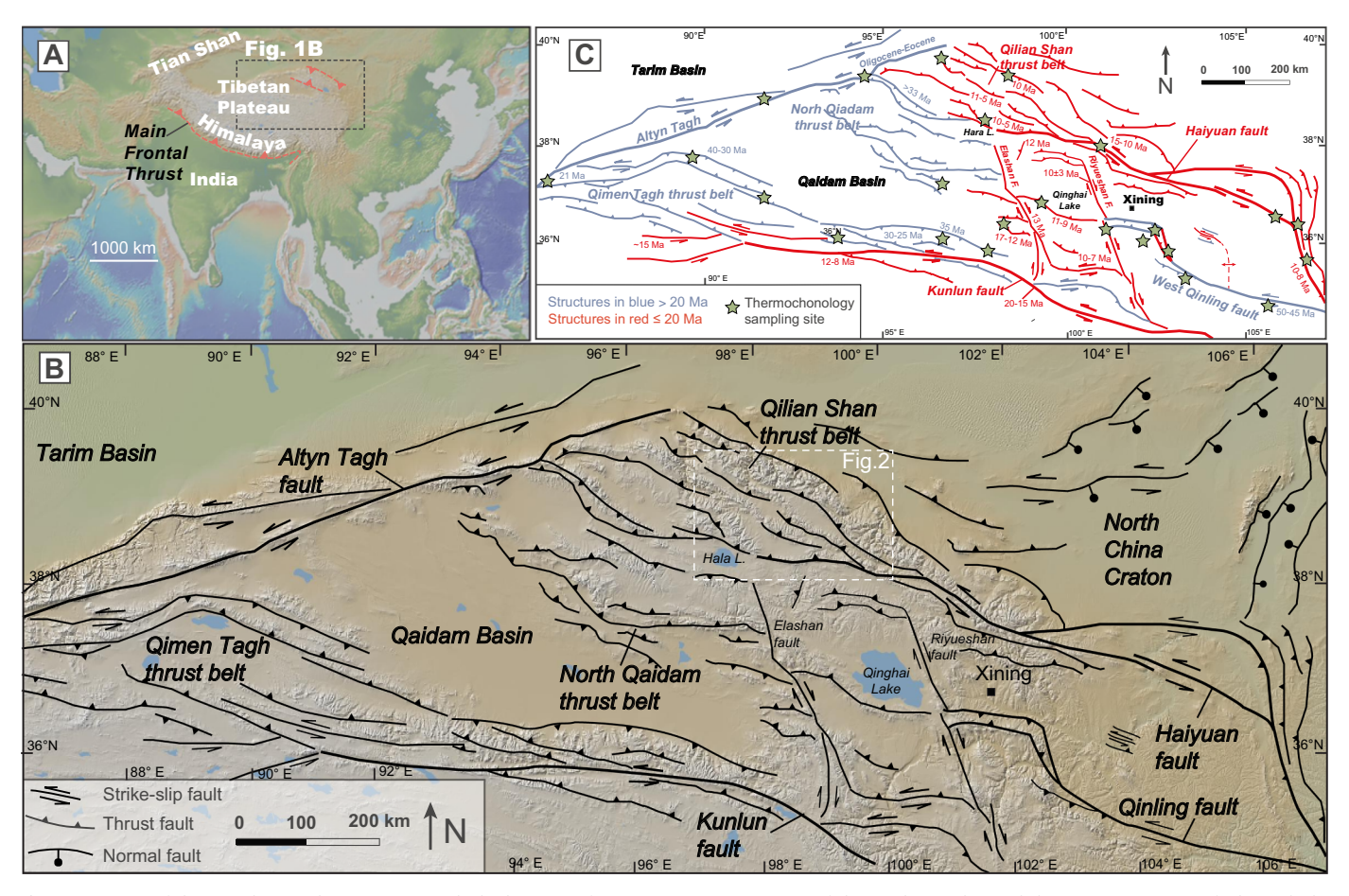


Fig. 1. (A) Map of the Himalayan-Tibetan orogen with the location of Fig. 1B. (B) Tectonic map of the northern Tibet and the primary Cenozoic faults with the location of detailed geologic map (Fig. 2). Cenozoic structures are from Taylor and Yin (2009), Duvall et al. (2013), and Zuza and Yin (2016). (C) Published thermochronology data (shown with green stars) of major Cenozoic structures across northern Tibet. Figure is modified from Duvall et al. (2013), Yuan et al. (2013), Zuza et al., (2019) and Wu et al. (2019a, 2019b). Cooling ages come from a variety of sources discussed in the text. (For interpretation of the references to colour in this figure legend, the reader is referred to the web version of this article.)

et al., 2004; Clark et al., 2010; Duvall et al., 2011; Clark, 2012; Yuan et al., 2013; Qi et al., 2016; Yu et al., 2017; Zhuang et al., 2018; An et al., 2020), but exposures of extensive thrust-fault-bounded Neogene-Quaternary basins and a strong ca. 15 Ma low-temperature thermochronology cooling signal suggest many of the present-day ranges are associated with middle to late Miocene shortening and exhumation (Fang et al., 2005; Zheng et al., 2006, 2010, 2017; Lease et al., 2012a, 2012b, 2007; Craddock et al., 2011; Hough et al., 2011; Zhang et al., 2012; Zhuang et al., 2011; Duvall et al., 2013; Yuan et al., 2013; Zuza et al., 2018; Li et al., 2019; Yu et al., 2019). The relatively low erosion rates and limited exhumation magnitude in northern Tibet hinders applications of thermochronology to systematically document fault activity (e.g., Zuza et al., 2019), leading to an incomplete kinematic framework for the northern Tibet.

To address the above issue and explore the spatial-temporal relationships between Eocene and Miocene to present deformation, we have conducted systematic geologic mapping, field observations, and apatite fission track (AFT) thermochronology across the central and northern Qilian Shan. We focused on pre-Cenozoic bedrock and Miocene sediments in fault-bounded ranges and basins, respectively, to elucidate the cooling history of this region. We document a complex history of overprinting thrust and strike-slip faulting since the early Cenozoic and present a kinematic model of the evolution of the northern Tibetan Plateau. We argue the Qilian Shan thrust belt progressed via out-of-sequence deformation starting in the Eocene, and the basins and ranges across the northern Tibetan Plateau have since experienced multiple phases of growth.

2. Regional geology

The Qilian Shan thrust belt, presently located > 1500 km north of the Himalayan collision front, defines the modern northeastern margin of the Tibetan Plateau between the Hexi Corridor to the north and the Qaidam Basin to the south, respectively (Fig. 1). The thrust belt experienced a complex tectonic history, including Neoproterozoic magmatism and deformation (Wu et al., 2017; Zuza et al., 2018), early Paleozoic orogeny (e.g., Xiao et al., 2009; Song et al., 2013, 2017; Zuza et al., 2018), Jurassic-Cretaceous extension with postulated Early Cretaceous contraction (e.g., Chen et al., 2003, 2004, 2019a; Yin et al., 2008a, 2008b; Zuza et al., 2016a, 2018), and Cenozoic deformation consisting of folding, thrusting, and strike-slip faulting to accommodate far-field India-Asia convergence (Tapponnier et al., 2001; Duvall et al., 2013; Yuan et al., 2013; Li et al., 2019).

2.1. Pre-Cenozoic tectonic evolution

Prior to the Cenozoic, the northeastern Tibetan Plateau experienced the early Paleozoic Qilian Orogen, which resulted from the Ordovician-Silurian closure of the Qilian Ocean(s) (e.g., Yin and Nie, 1996; Yin and Harrison, 2000; Gehrels et al., 2003a; Yin et al., 2007a, 2007b; Song et al., 2013, 2017; Wu et al., 2017; Zuza et al., 2018) during progressive southward/bi-directional subduction and related arc magmatism (e.g., Cowgill et al., 2003; Gehrels et al., 2003a, 2003b; Su et al., 2004; Hu et al., 2005; Wu et al., 2006, 2010; Liu et al., 2006; He et al., 2007; Tseng et al., 2009; Xia et al., 2012; Xiong et al., 2012; Song et al., 2013;

Wu et al., 2016; Zuza et al., 2018; Chen et al., 2019b). Ultimate continental collision resulted in three suture zones (i.e., the North, Middle and South Qilian suture zones, Song et al., 2017, 2019) although these dismembered exposures may be subsequently duplicated by the Cenozoic shortening (Yin et al., 2007b; Zuza et al., 2018). This orogen, composed of Neoproterozoic to Early Paleozoic ophiolitic mélange, Ordovician–Silurian volcanic rocks and granitoid plutons, Silurian turbidite sequence, Devonian conglomerate, and post-orogenic Carboniferous to Triassic marine sediments makes up the majority of bedrock of the modern Qilian Shan.

The Qilian Shan experienced Jurassic-early Cretaceous regional extension (e.g., Chen et al., 2003, 2004; Yin et al., 2007a; He et al., 2019), and deposition of Jurassic-Cretaceous terrestrial sedimentation along east-trending extensional and transtensional structures (e.g., Vincent and Allen, 1999; Chen et al., 2003, 2004; Yin et al., 2008b; Zuza et al., 2018; He et al., 2019). This area may have underwent a pulse of Early Cretaceous contractional deformation, which resulted in the onset of thrusting and development of growth strata in northern Tibet (Chen et al., 2019a; He et al., 2019). Previous low-temperature thermochronology studies have revealed this Early Cretaceous pulse of exhumation that may be related to the localized shortening (e.g., Jolivet et al., 2001; Qi et al., 2016; Li et al., 2019).

2.2. Cenozoic structures and range growth

The Cenozoic Qilian Shan thrust belt is comprised of thrust and strike-slip faults, which have accommodated India-Asia convergence at the northeast margin of the Tibetan Plateau (Vincent and Allen, 1999; Tapponnier et al., 2001; Yin et al., 2007a, 2008a, 2008b; Duvall et al., 2013; Yuan et al., 2013; Zuza and Yin, 2016; Zuza et al., 2016a; Li et al., 2019). Cenozoic deformation and range growth in the southern Qilian Shan and the North Qaidam thrust belts, locally initiated by 50-40 Ma shortly after the India-Asia collision (e.g., Jolivet et al., 2001; Spurlin et al., 2005; Jiang et al., 2008; Wang et al., 2008; Zhuang et al., 2011; Qi et al., 2016). Deformation appears to have propagated nearly simultaneously northward to the northern Qilian Shan and southward to the Qimen Tagh thrust belts starting in the early Miocene (George et al., 2001; Jolivet et al., 2001; Dupont-Nivet et al., 2004; Yin et al., 2008a, 2008b; Duvall et al., 2011; Yuan et al., 2013; Zheng et al., 2017; Li et al., 2019; An et al., 2020). This pulse of Miocene accelerated regional deformation across the Qilian Shan resulted in the development of major thrust and strike-slip faults (e.g., Zheng et al., 2006, 2010, 2017; Duvall et al., 2013; Yuan et al., 2013; Zuza and Yin, 2016; Allen et al., 2017; Li et al., 2019; Yu et al., 2019) (Fig. 1). Miocene deformation was accompanied by related rapid exhumation and range growth and the formation of a major geomorphic boundary between the plateau and its northern foreland in northern Tibetan Plateau.

Drawing from earlier models of northward propagation of the Tibetan Plateau (e.g., England and Houseman, 1986; Tapponnier et al., 2001), this recent pulse of Miocene range exhumation has been related to a simple northward progression of thrust-system development in the northern Tibet (e.g., Zheng et al., 2010, 2017; Su et al., 2019; Yu et al., 2019). However, existing evidence for early Cenozoic deformation, including Eocene-Oligocene cooling ages distributed across the Qilian Shan and localized early Cenozoic basin strata (e.g., Dai et al., 2005, 2006; Yin et al., 2008a, 2008b; Zhuang et al., 2011; Clark, 2012; Qi et al., 2015, 2016; Yu et al., 2017; He et al., 2018; Jia et al., 2018; Cheng et al., 2019a, 2019b), suggests a more complex evolution history. We focus this study on the central and northern parts of the Qilian Shan thrust belt, where our new observations provide valuable insight on kinematic models in the northern Tibet of either progressive northward range growth or multi-phase overprinting exhumation since the early Cenozoic. The study area consists of four major west-trending ranges: the Shule Nan Shan, Tuolai Nan Shan, Tuolai Shan and North Qilian Shan ranges, from south to north, respectively (Fig. 2).

2.3. Structural geology

Structures in the Qilian Shan primarily trend northwest, expressed by the strike of major range-bounding faults and folds, and overall trend of the dominant ranges. A mylonitic gneiss complex exposed in the hanging wall of the Shule Nan Shan, Tuolai Nan Shan, and Tuolai Shan thrust faults also has northwest-striking foliations. The protolith of the gneiss is Proterozoic, and the complex was an Ordovician shear zone during the early Paleozoic Qilian orogen, as dated by crosscutting intrusions and in-situ monazite dating (Zuza et al., 2018). Brittle faults and folds within this complex merge with structures cutting younger Paleozoic-Mesozoic stratigraphy and present-day range-bounding thrusts. Accordingly, we interpret that most of the observed contractional structures are Cenozoic in age, although they may reactivate older early Paleozoic structures. In some localities, Paleozoic-Mesozoic strata are thrusted over Cenozoic terrestrial sediments (Fig. 3A–C).

Muli basin, which is enriched with Triassic-Jurassic coal, bounds the southeastern of the Tuolai Nan Shan (Fig. 2). Here, we observe Eocene strata thrust over Neogene sandstone (Fig. 3D). The Qilian Shan has a broad planation surfaces at 3000–3200 m, indicative of tectonic uplift of the Tibetan Plateau (Cui et al., 1997; Li and Fang, 1999; Zhou et al., 2006; Jia et al., 2018). Planation surface developed on the top of tilted Eocene red-beds in the north of Muli basin, and were later incised by Datong River (Fig. 3E). In Suli Basin, reddish brown Miocene sediments are tilted northeast with dip of 25° (Figs. 2, 3F).

The east-striking left-slip Haiyuan fault is geometrically and kinematically connected with the central Qilian Shan thrust belt to the west (Figs. 1, 2) (Cheng et al., 2015; Zuza et al., 2016b, 2018; Li et al., 2019). Specifically, the western segment of the Haiyuan fault, transferring into the Shule Nan Shan thrust system, is located within our study region, where strike-slip displacement appears to transfer into primarily dipslip thrust faulting (Fig. 2). We observed from satellite images that the western Haiyuan fault termination is a relatively active structure, cutting and offsetting Quaternary alluvial fans (Fig. 4).

3. Methods

Low-temperature thermochronology enables quantification of the timing and rates at which rocks cool and approach the surface during exhumation, which can be interpreted to constrain the cooling history and timing of major fault activity (e.g., Dodson, 1973; Clark et al., 2010; Zheng et al., 2010, 2017; Curry et al., 2016; Li et al., 2019; Yu et al., 2019). The AFT dating method is based on crystallographic damage trails due to the constant-rate spontaneous nuclear fission of trace levels of $^{238}\rm{U}$ in apatite grains (e.g., Wagner, 1968; McDannell et al., 2019). Crystal damages in apatite are incompletely annealed through the partial annealing zone (PAZ, Gleadow, 1981; Ketcham et al., 2007) in between the temperature zone of $\sim\!60-110$ °C. The thermal history that a rock sample has experienced through the PAZ can be reflected by track length distribution.

During deformation, rocks at originally different structural levels will exhume toward the surface and thus cool at different rates, depending on their relationships to major structures. Thermochronologic analysis of minerals from bedrock samples thus requires careful consideration of the structures that are responsible for cooling, especially when interpreting different cooling signals. Fission track analysis on detrital apatite grains from basin sediments is a commonly used method for reconstructing and quantifying the long-term exhumation history and trace their deposits age variation. Applying AFT dating on in-situ bedrock samples and detrital basin sediments allows for complete evaluation of source area's thermal evolution and exhumation history.

In this study, we conducted two broad sampling traverses across major thrust structures near the western segment of the Haiyuan fault across the central and northern Qilian Shan (Fig. 2). Previous lowtemperature thermochronology study in this region derived Early Cretaceous and late Miocene rapid cooling ages, which reflect relatively

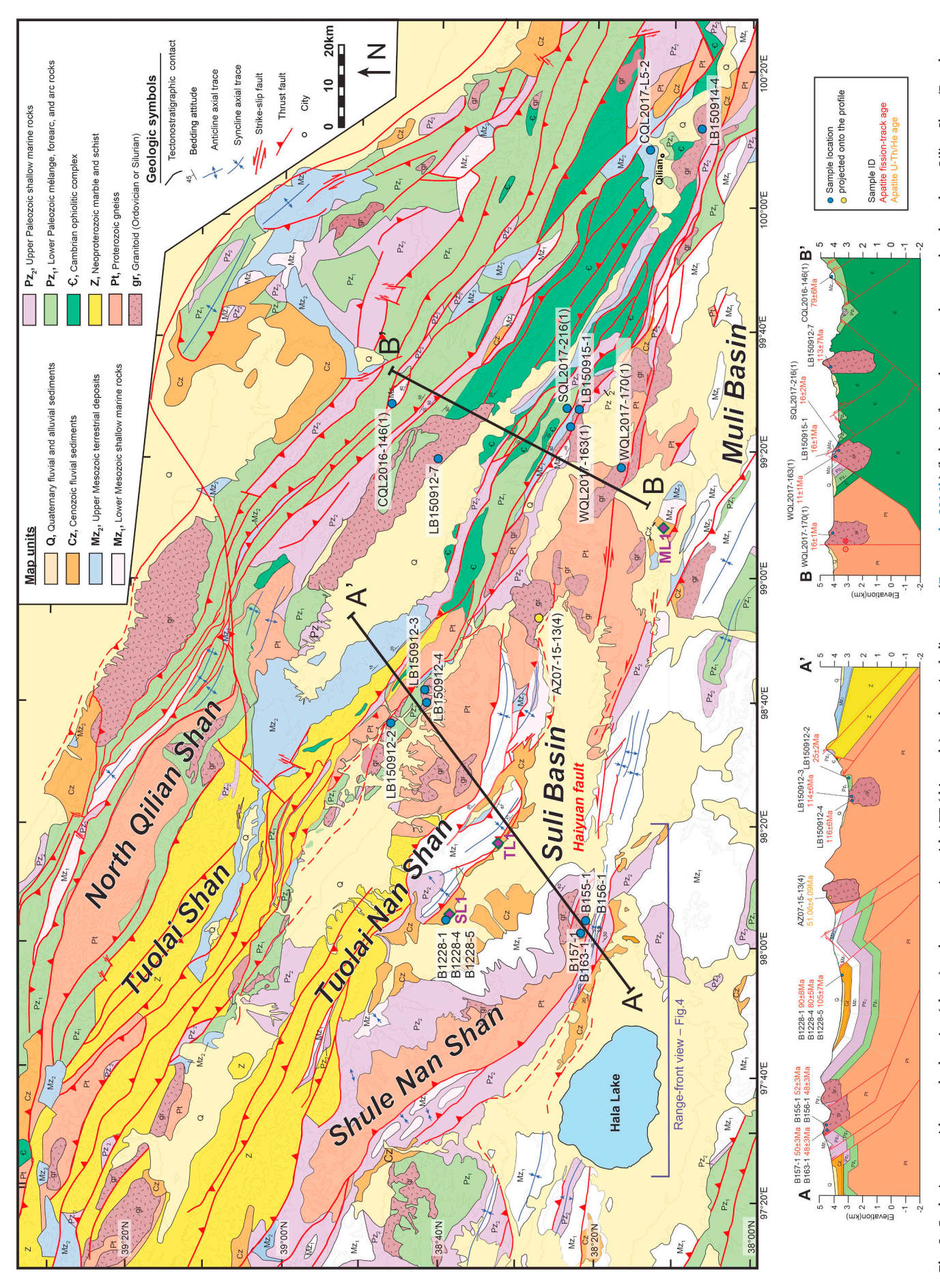


Fig. 2. Geologic map with samples location (above) and cross section with AFT (this study) and apatite helium ages (Zuza et al., 2016b) (below) of samples across the central and northern Qillian Shan (Based on our geologic mapping and Zuza et al., 2013, 2018). Annotations TL1, ML1 and SL1 correspond to field sites discussed in this study.

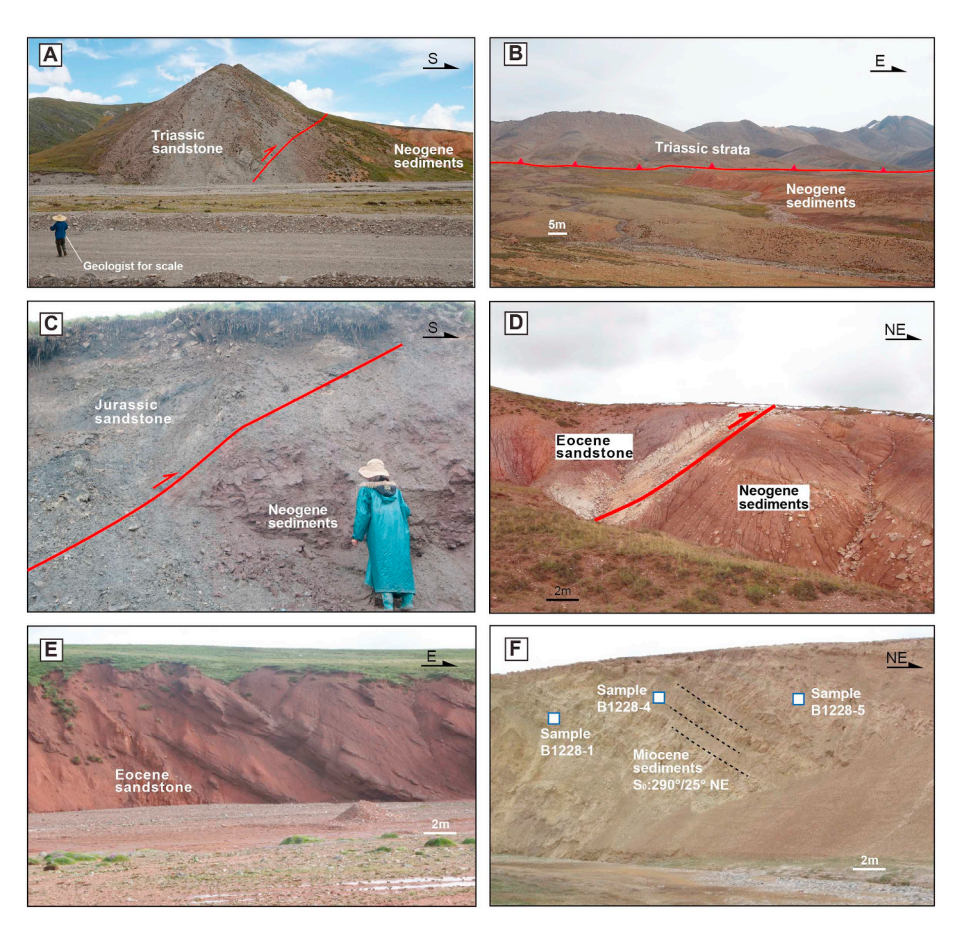


Fig. 3. Field photographs from the central and northern Qilian Shan. (A–C) South-directed thrust faults place Triassic/Jurassic strata over Neogene sediments; photo was taken at TL1 in Fig. 2. (D) Southdirected thrust faults placed Eocene strata over Neogene sediments. (E) Planation surface developed on the top of tilted Eocene strata; photo was taken at ML1 in Fig. 2. (F) Tilted Miocene sediments in Suli Basin with samples location; photo was taken at SL1 in Fig. 2.

limited exhumation and long residence in PAZ (e.g., Zheng et al., 2017; Zuza et al., 2016b; Yu et al., 2019). We collected and analyzed eighteen AFT samples as part of two different sampling approaches: (1) fifteen in-situ bedrock samples from hanging wall and footwall of major range-bounding thrust faults, respectively; and (2) three detrital sedimentary samples collected from Cenozoic sediments in the Suli Basin. For our bedrock samples, we describe the hanging wall and footwall samples separately because of their different structural positions and they yield significantly distinct age populations. Rock samples consist of Cambrian-Ordovician granite and granodiorite (Wu et al., 2017), Mesozoic sandstone, and Miocene sediments. Detailed lithology and location information of each sample are presented in Table 1.

3.1. AFT analysis

Apatite grains in this study were separated from whole-rock samples using standard magnetic and heavy-liquid separation methods at the Hebei Institute of Geology and Mineral Resources in China. Apatite grains were first mounted in epoxy resin on glass slides and then polished to expose the internal grain surface. Spontaneous tracks in the apatite grains were revealed by etching using 5.5% HNO $_3$ for 20s at 21 °C. Low-uranium (< 4 ppb) muscovite grains as external track detectors were packed together with apatite grain mounts and CN5 uranium glass dosimeters were irradiated in the well thermalized hotneutron flux in the 492 Swim-Pool nuclear reactor at China Institute of Atomic Energy, Beijing. Muscovite detectors were taken off and etched in 40% HF for 20 m at 25 °C to reveal the induced fission tracks (Yuan et al., 2003). Track densities for both spontaneous and induced fission

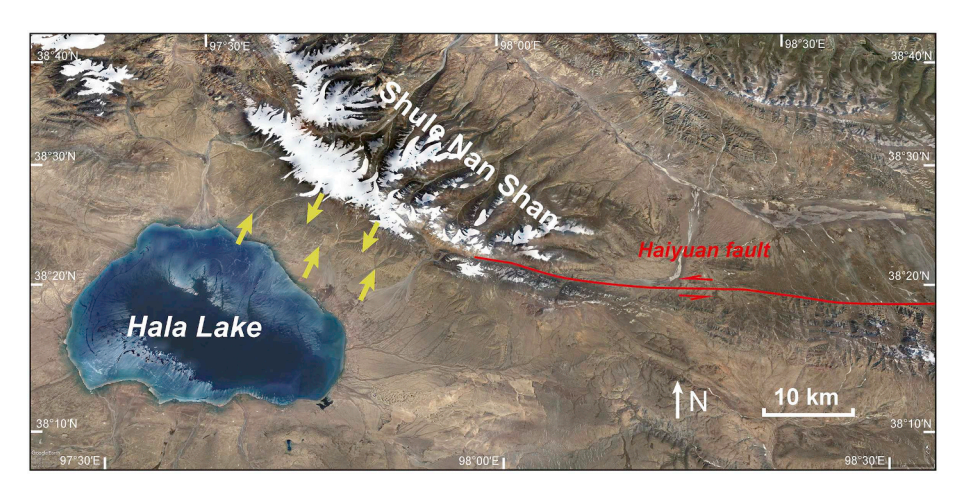


Fig. 4. Northward-looking view of Shule Nan Shan rangefront; image from Google Earth. Yellow arrows point to a thrust fault bounding the range that crosscuts active alluvial fans. This thrust system represents the western termination of the left-slip Haiyuan fault. See **Fig. 2** for location. (For interpretation of the references to colour in this figure legend, the reader is referred to the web version of this article.)

Table 1 Summary of AFT samples.

Sample ID	Lat. (°N)	Long. (°E)	Elevation (m)	Geologic time	Description
Samples from foot wall of	bedrock				
LB150912-3	38°42′26.0″	98°38′59.5″	3589	Ordovician	Granite
LB150912-4	38°41′49.4″	101°50′20.9″	3546	Ordovician	Granite
LB150912-7	38°38′23.1″	99°20′08.4″	3488	Cambrian	Granite
Samples from hanging wal	ll of bedrock				
CQL2016-146(1)	38°46′15.6″	99°27′39.9″	2708	Triassic	Sandstone
B155-1	37°42′11.2″	101°54′22.8″	4332	Ordovician	Granodiorite
B156-1	37°49′34.9″	102°00′39.7″	4382	Ordovician	Granodiorite
B157-1	37°38′28.0″	101°50′16.6″	4368	Ordovician	Granite
B163-1	37°44′01.4″	101°56′00.8″	4344	Ordovician	Granite
LB150914-4	38°07′23.4″	100°11′28.5″	3128	Ordovician	Granite
LB150912-2	38°45′57.0″	98°37′40.8″	3712	Ordovician	Granite
CQL2017-L5-2	38°12′50.7″	100°08′55.8″	2791	Cretaceous	Sandstone
SQL2017-216(1)	38°22′58.9″	99°27′16.3″	3364	Ordovician	Gabbro
LB150915-1	38°22′44.7″	99°26′58.5″	3401	Ordovician	Diorite
WQL2017-170(1)	38°17′14.4″	99°18′03.4″	3877	Ordovician	Granite
WQL2017-163(1)	38°23′5.9″	99°23′54.5″	3819	Ordovician	Granite
Samples from detrital sedi	mentary rocks				
B1228-1	38°39′03.2″	98°06′13.5″	3760	Miocene	Sandstone
B1228-4	38°39′03.2″	98°06′13.5″	3764	Miocene	Sandstone
B1228-5	38°39′03.2″-13.2″	98°06′13.5″	3768	Miocene	Sandstone

Explanation and source

Table 2 Thermal history model input table for simulations of central and northern Qilian Shan apatite fission track data.

1. Apatite fission track data
Samples and data used in simulations

Data type	Data source

AFT singe grain ages and individual

track lengths

Data treatment, uncertainties, and other relevant constraints

Treatment: each of bedrock samples was conducted as a separated constraint in HeFTy

Error (Ma) applied in modeling: the 1σ sample standard deviation of each sample was applied

This study (Supplemental File, Tables S1 and S2)

2. Additional geologic information

Initial condition begin at high temperature of 160-200 °C

Available AFT data indicated complete apatite annealing at this high temperature AFT ages was set through the apatite PAZ temperature range of 60–110 °C The AFT system is especially sensitive to this temperatures range (~60-110 °C, Gleadow and Duddy,

Note: deposit age was used as the initial condition at the surface temperature for sample CQL2017-L5-2.

1981) At surface temperature of 20 ± 5 °C by 0 Ma Average surface temperature is endmember minimum estimate.

3. System-and model-specific parameters

Modeling Code: HeFTy v1.9.1

FT annealing model: Multi-kinetic annealing model of Ketcham et al. (2007); the Dpar values and the angle with C-axis parameters were applied Statistical fitting criteria: GOF values > 0.05 for accepted fit; GOF values > 0.5 for good fit;

Number of t-T paths attempted: 10000 for each sample

t-T path characteristics: reheating allowed after AFT age.

tracks were measured with a dry objective magnification. All ages were calculated using zeta calibration approach (Hurford, 1990) with a zeta value of 391 \pm 17.8 for CN5.

The chi-square (χ^2) test was used to detect the probability of all analyzed age grains belonging to a single population (Galbraith, 1981). If single grain ages have χ^2 test results of < 5%, the sample is an asymmetric spread of single-grain ages. Accordingly, a conventional analysis based on the Poisson-variation (Green, 1981) is invalid and the central age is clearly not appropriate for mixed populations, in that it provides only an average age for all grains. The method of binomial "peak-fitting" by Galbraith and Green (1990) and Galbraith and Laslett (1993) was applied by RadialPlotter program (Vermeesch, 2009) to decompose the AFT singe grain age into a radial plot of component distributions, and to interpret the results using the average ages for those components.

To define the chemical composition of the apatite affecting the characteristics of the annealing process, we also measured the maximum diameter of fission track etch pit parallel with crystallographic Caxis (Dpar). Horizontal confined fission track lengths were measured on a cylinder with parallel C-axis (Green et al., 1986).

3.2. Thermal modeling

Thermal history modeling of the bedrock samples was conducted using the HeFTy program (Ketcham, 2005) considering the fission-track parameters and the geological background. The inversion models were

Table 3Apatite fission track analyzed results of bedrock samples from the central and northern Qilian Shan.

Sample ID	N	ρ_s (N _s)	ρ_i (N _i)	ρ_d (N _d)	$P(\chi^2)$	Age	MFTL	No. tracks	Average Dpar
		$(10^5/\text{cm}^2)$	$(10^5/\text{cm}^2)$	$(10^5/\text{cm}^2)$	(%)	(Ma ± 1σ)	(μm ± 1σ)		(μm)
LB150912-3	32	10.374(2883)	16.704(4642)	9.052(6313)	6.5	114 ± 6	11.4 ± 1.8	101	1.69
LB150912-4	34	4.117(1763)	6.261(2681)	8.671(6313)	22.9	116 ± 6	12.3 ± 1.8	112	1.72
LB150912-7	35	10.553(1914)	16.012(2904)	8.29(6313)	0	113 ± 7	13.2 ± 1.8	103	1.75
CQL2016-146(1)	35	3.753(397)	13.255(1402)	13.734(6039)	86.7	79 ± 6	11.5 ± 2.0	96	2.07
B155-1	35	8.381(1674)	29.222(5837)	9.002(6788)	0	52 ± 3	13.1 ± 1.8	118	2.32
B156-1	35	7.297(1289)	30.123(5321)	9.733(6788)	10.4	48 ± 3	12.7 ± 2.0	120	2.08
B157-1	35	6.573(1680)	28.488(7281)	10.672(6788)	1.3	50 ± 3	13.0 ± 1.9	105	2.43
B163-1	35	8.042(1166)	31.822(4614)	9.315(6788)	10.7	48 ± 3	12.8 ± 2.3	105	2.08
LB150914-4	30	10.717(4271)	45.176(18003)	7.908(6313)	0	39 ± 2	11.6 ± 1.9	107	1.83
LB150912-2	35	2.502(366)	19.464(2847)	9.434(6313)	7.1	25 ± 2	11.8 ± 2.6	101	-
CQL2017-L5-2	35	0.672(252)	5.91(2215)	9.378(5949)	95.7	21 ± 2	12.7 ± 2.1	102	1.53
SQL2017-216(1)	35	2.2(511)	19.976(4640)	7.753(5949)	0	16 ± 2	12.2 ± 2.0	104	1.63
LB150915-1	35	8.432(1637)	79.406(15416)	7.527(6313)	0	16 ± 1	11.6 ± 2.5	101	1.76
WQL2017-170(1)	35	0.899(199)	8.971(1985)	8.403(5949)	100.0	16 ± 1	13.1 ± 1.9	82	1.77
WQL2017-163(1)	35	0.731(183)	9.801(2452)	7.753(5949)	100.0	11 ± 1	$12.9 ~\pm~ 2.0$	101	1.57

N: number of analyzed apatite grains; $\rho_s(N_s)$: spontaneous track density (number); $\rho_i(N_i)$: induced track density(number); $\rho_d(N_d)$: track density measured in glass dosimeter (number); MFTL: mean fission-track length; No. tracks: number of measured apatite fission tracks lengths; (-): not analyzed.

run with single grain ages and observed track lengths for each sample. Goodness-of-fit (GOF) value was used to estimate how well the modeled data fit measured values (Ketcham, 2005). The thermal history model inputs for simulations are in Table 2 (Flowers et al., 2015).

4. Results and Interpretations

4.1. Apatite fission track results

The results of AFT analyses from bedrock samples are shown in Table 3, including AFT age, track length, and Dpar information. AFT ages from fifteen bedrock samples spread in range from 116 ± 6 Ma (sample LB150912-4) to 11 \pm 1 Ma (sample WQL2017-163(1)). All the analyses are significantly younger than their respective crystallization or depositional ages (Table 1). Results from nine of the bedrock AFT samples passed the chi-square test (P (χ^2) > 5%; Fig. 5A) and six of the bedrock samples (i.e., LB150912-7, B155-1, B157-1, LB150914-4, SQL2017-216(1) and LB150915-1; Table 3) failed the chi-square test (P (χ^2) < 5%; Galbraith and Green, 1990). On single grain radial plots, four of these samples have age dispersions $\leq 21\%$, which suggests the age dispersion are possibly caused by some single discordant grain ages (Fig. 5B), rather than multiple AFT age populations. For the two samples with age dispersion of 39% and 42%, respectively, the age dispersion may result from (1) existing strongly annealed and shortened fission tracks causing difficulties in accurate identification of these tracks (e.g., Gleadow et al., 1986; Green, 1988; Lin et al., 2011; An et al., 2020) and/or (2) chemical composition variation of apatite grains in a single sample (e.g., Galbraith and Laslett, 1993; O'Sullivan and Parrish, 1995). We used the central age of these samples, and for the remaining AFT samples that passed the chi-square test, pooled AFT ages are reported (e.g., Sobel et al., 2006a, 2006b). The variable single grain ages of the AFT samples can be also observed in some other region of the northern Tibet (Craddock et al., 2014; Zheng et al., 2017; He et al., 2018; Li et al., 2019; Yu et al., 2019; An et al., 2020).

Thrust footwall samples yield AFT ages that are \geq 113 Ma (Fig. 5), implying that the Paleozoic granites from the central and northern Qilian Shan have been thermally and tectonically stable since the Cretaceous. Samples from the hanging wall of range-bounding thrusts have Cenozoic AFT ages, younger than ca. 52 Ma, with a exception of sample CQL2016-146(1) with an AFT age of 79 \pm 6 Ma (Fig. 5A; Table 2). These AFT ages suggest that samples have experienced post-crystallization or post-depositional cooling histories through the apatite PAZ (Galbraith and Laslett, 1993; Gallagher et al., 1998; Yuan et al., 2006). AFT age distribution of all the bedrock samples is corresponding

with their structural positions (Fig. 2). The mean track lengths of AFT bedrock samples ranges from 11.4 \pm 1.8 μm (sample LB150912-3) to 13.2 \pm 1.8 μm (sample LB150912-7) (Table 3). The vast majority of apatite track length distributions are between 11 and 12 μm , which suggests that track lengths in most of the samples have been shortened by annealing and indicates the samples have been experienced long-term annealing-related residence in the PAZ, Dpar values are slightly variable in the analyzed samples, ranging from 1.53 to 2.43 (Table 3). The dispersion of Dpar values maybe due to a bias in the data collection for the granitic rocks and heterogeneous chemical composition of the sandstones (e.g., Craddock et al., 2014; Li et al., 2019).

4.2. Detrital AFT results

The three detrital samples are from Miocene sediments of Suli Basin (Fig. 3F). The AFT analyses are presented in Table 4, and all samples exhibit a respectively wide range of AFT ages (Fig. 6A, Table 4). Sample B1228-1 exhibits a weighted mean AFT age of 90 ± 8 Ma with four age peaks (early Cretaceous age of 130.3 ± 5.0 Ma, late Cretaceous age of 84.4 ± 4.8 Ma, early Eocene age of 51.5 ± 3.5 Ma and late Eocene age of 36.1 \pm 4.2 Ma). Sample B1228-4 shows a weighted mean AFT age of 80 \pm 5 Ma with three age peaks (early Cretaceous, 111.0 \pm 20.0 Ma; late Cretaceous age, 85.0 \pm 10.0 Ma; and early Paleocene, 63.3 ± 7.2 Ma). Sample B1228-5 yields weighted mean AFT age of 105 ± 7 Ma with two age population of early Cretaceous age of 116.0 \pm 3.6 Ma and late Cretaceous age of 98.2 \pm 7.8 Ma (Fig. 6A; Table 4). The mean track lengths of these three detrital AFT samples ranges from 12.9 \pm 1.8 μ m (sample B1228-1; n = 118) to 13.4 \pm 1.6 μ m (sample B1228-5; n = 100) (Table 3). Dpar values in the analyzed apatite grains are with an average value extending from 1.83 to 2.43 μm (Table 4).

We combined the 100 detrital AFT grain ages from these three Miocene sedimentary rocks into a single dataset and used Radial Plotter program (Vermeesch, 2009) to evaluate discrete AFT age populations (Fig. 6B). Four AFT age populations are observed in the diagram with age peaks of 135.8 \pm 7.6 Ma, 91.4 \pm 8.5 Ma, 63.5 \pm 6.6 Ma and 50.0 \pm 8.2 Ma, respectively, which demonstrates the multi-phase rapid cooling affected the central and northern Qilian Shan since early Cretaceous to early Cenozoic (Fig. 6B). Sample CQL2017-L5-2 from Cretaceous strata of northern Qilian Shan yields a dominant AFT age peak in Miocene age of 18.7 \pm 1.5 Ma with some subordinate age components (Fig. 6C).

4.3. Thermal modeling

As the apparent AFT age may not directly relate to specific geological event in a complex cooling/tectonic history (e.g., Gleadow and Brown, 2000), thermal history modeling of the AFT ages and track lengths is useful to further evaluate the cooling processes. We conducted thermal history modeling of all bedrock samples to explore the denudation history of the central and northern Qilian Shan.

Three bedrock samples collected from footwall locations yielded Cretaceous AFT ages. Modeling of these samples reveals cooling in the late Jurassic to early Cretaceous to the bottom of the AFT PAZ, followed by thermal stagnation in the PAZ and accelerated cooling at ca. 20 Ma

to the surface (Fig. 7A).

Twelve bedrock AFT samples collected from hanging wall locations show more variable cooling histories than the aforementioned footwall samples. Sample CQL2016-146(1) from the hanging wall of the North Qilian thrust fault experienced Early Cretaceous rapid cooling, subsequent long-term tectonic quiescence in the PAZ, and accelerated cooling to the surface at ca. 10 Ma. Samples B155-1, B156-1, B157-1 and B163-1 from near Shule Nan Shan thrust fault and sample LB150914-4 from Tuolai Shan thrust fault underwent a strong pulse of rapid cooling at ca. 55 Ma, and a final phase of Miocene cooling. Time-temperature models for samples LB150912-2 and LB150915-1 from Tuolai Shan thrust fault suggest a reheating event affected the samples.

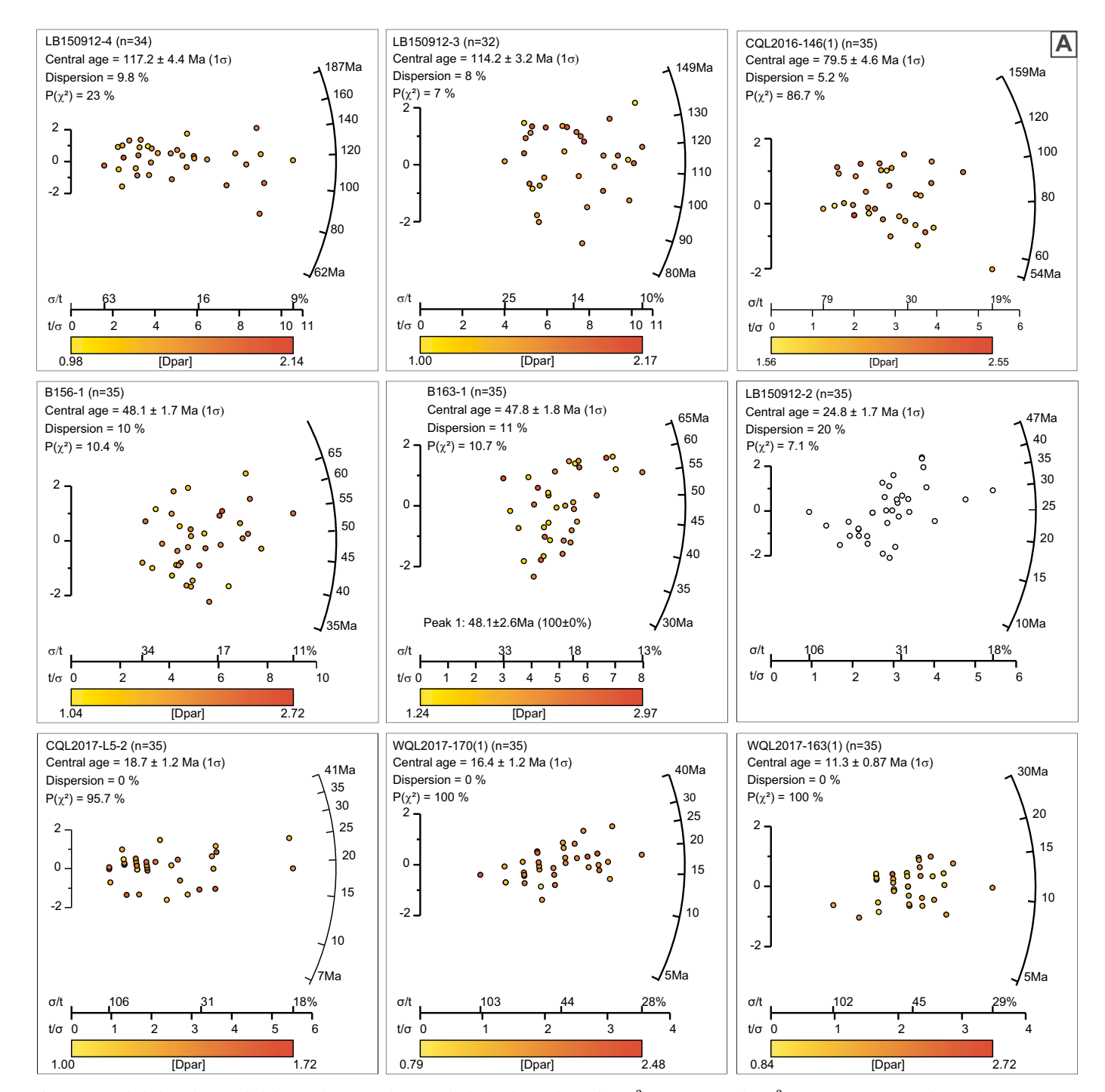


Fig. 5. AFT radial plots (from RadialPlotter of Vermeesch, 2009) for bedrock samples with $P(\chi^2) > 5\%$ (A) and $P(\chi^2) < 5\%$ (B), respectively. Single-grain ages are statistically split into two populations (Peak 1 and Peak 2) if $P(\chi^2) < 5$ of samples.

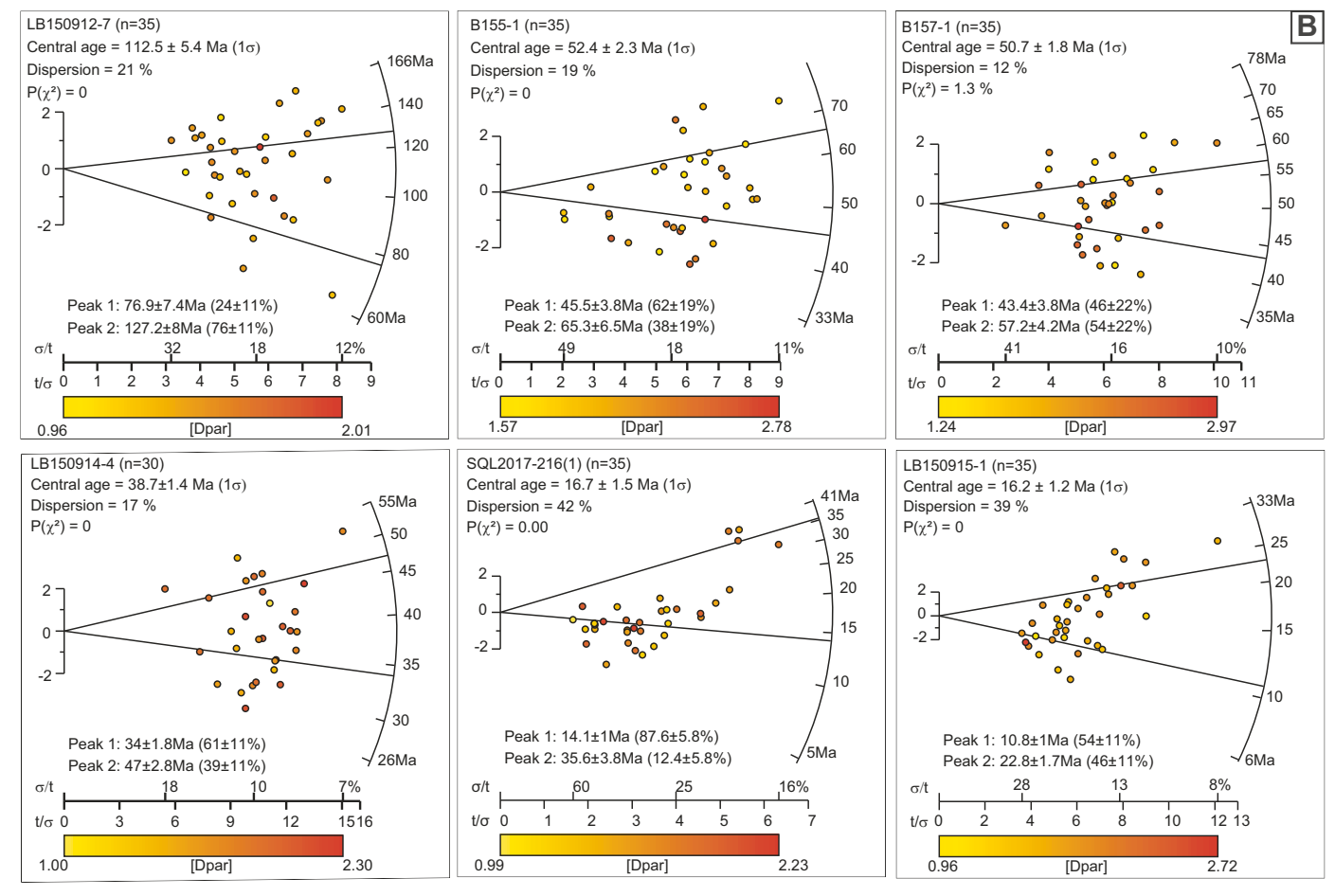


Fig. 5. (continued)

Specifically, these samples show cooling to the PAZ by the Eocene, reheating at ca. $\sim\!30\text{--}25$ Ma, and final ca. 10 Ma cooling. This history is supported by the tracks length information that show a wide and bimodal distribution with a significant population with relatively short track lengths ($\leq\!10~\mu\text{m}$) (Fig. 7B; Table 4), which may result from incomplete annealing of fission tracks during reheating of the samples within the PAZ. The remaining four hanging wall bedrock samples (CQL2017-L5-2, SQL2017-216(1), WQL2017-163(1) and WQL2017-170(1)) show Oligocene fast cooling with a pulse of final cooling since ca. 10 Ma (Fig. 7B).

5. Discussion

5.1. Thermal and tectonic history of the central and northern Qilian Shan

AFT analyses and thermal modeling suggest that the central and northern Qilian Shan experienced a complex multi-phase cooling history through early Cretaceous to the present-day (Figs. 7, 8). Samples

from footwall bedrock yield older AFT ages (Table 3). Their thermal models suggest a period of Jurassic to Cretaceous cooling and slow exhumation over the Cenozoic, which indicate that these samples may have experienced long-term residence in the apatite PAZ through the late Cretaceous to Cenozoic. Similar observations have been made elsewhere in the Qilian Shan (e.g., George et al., 2001; Pan et al., 2013; Qi et al., 2016; Li et al., 2019). Bedrock samples from the hanging wall display a range of AFT ages (Table 3), and their modeled thermal histories are consistent with variable Cenozoic cooling. Several samples show bimodal and complicated track-length distributions that suggest phases of slight reheating, possibly due to thrust burial (Fig. 7B). Fig. 9 schematically shows how several phases of Cretaceous to present faulting-related exhumation may have resulted in our observed AFT ages and track lengths.

The first phase of local late Jurassic-early Cretaceous cooling (Fig. 8A) recorded by our AFT results of bedrock footwall and detrital samples suggests a period of regional exhumation, which is corresponding with other low-temperature thermochronology datasets

Table 4Detrital Apatite fission track analyzed results of Miocene sedimentary samples from Suli Basin.

Sample ID	N	$\rho_s \; (N_s)$	$\rho_i \; (N_i)$	ρ_d (N _d)	$P(\chi^2)$	Age	Mixture model peaks $\pm \sigma$ (Ma)			MTL (μm)(n)	Average	
		10 ⁵ /cm ²	$10^5/\mathrm{cm}^2$	$10^5/\mathrm{cm}^2$	(%)	(Ma ± 1σ)	P1	P2	Р3	P4	(μπ)(π)	Dpar (μm)
B1228-1 B1228-4	35	3.553(760)	11.136(2382)	12.295(6313)	4.7	90 ± 8 80 ± 5	63.3 ± 7.2	85 ± 10	$111.0 ~\pm~ 20$		12.9 ± 1.6(89)	2.09
B1228-5	35	2.304(789)	5.13(1757)	11.532(6313)	100	105 ± 7	98.2 ± 7.8	116.0 ± 3.6	-	-	$13.4 \pm 1.6(100)$	2.43

Single-grain ages are statistically split into peaks (P1–P4) using DensityPlotter (Vermeesch, 2012). Modeled peak ages (with estimated standard deviations) and proportions of age components are given. (-) indicates no data.

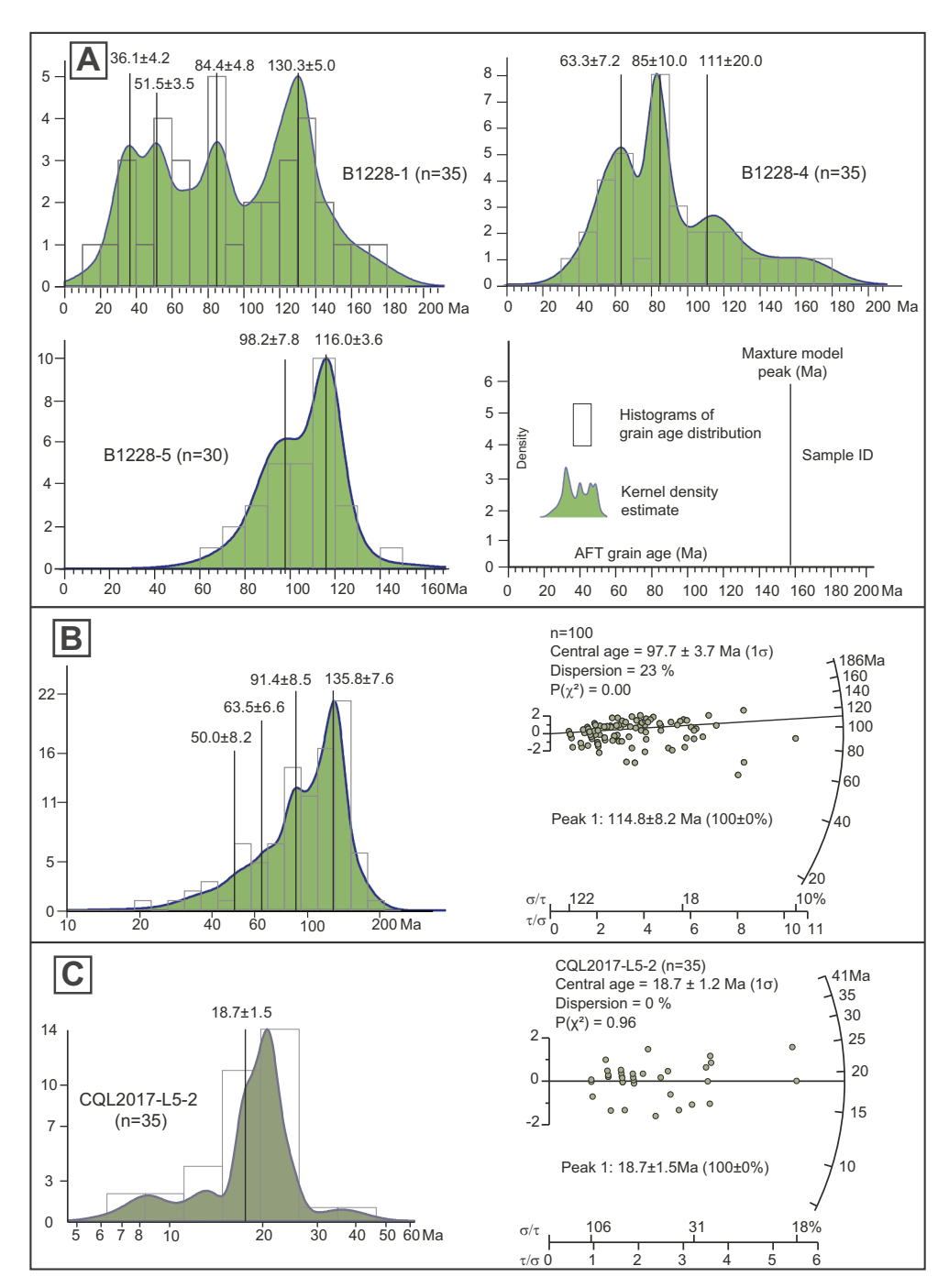


Fig. 6. (A) Grain-age distributions and kernel density estimates of AFT ages from three Miocene detrital samples. Probability grain-age distribution (left) and radial plots (right) of AFT analyses. (B) Combined analyses from the three detrital samples from Suli Basin and (C) Cretaceous sandstone of Sample CQL2017-L5-2. Single grain ages are statistically split into populations (P1-P4) using the routines in DensityPlotter (Vermeesch, 2012). The modeled means (with estimated standard deviations) and proportions of age components are shown.

across the Qilian Shan (Jolivet et al., 2001; George et al., 2001; Pan et al., 2013; Qi et al., 2016; Li et al., 2019) and stratigraphic records in northeastern Qaidam Basin (Ritts and Biffi, 2000; Cheng et al., 2019a, 2019b). This pulse of cooling may be related to the far-field effects of the closure of the Paleo-Tethys Ocean along the Kunlun-Anyemaqen suture zone (Pullen et al., 2008; Wu et al., 2017; Cheng et al., 2019a, 2019b) and the collision between the Lhasa Block and the Qiangtang Block along the Bangong-Nujiang suture zone during Middle Jurassic to early Cretaceous (Kapp et al., 2007; Gao et al., 2019). The exact driver of this regional exhumation remains unconstrained, but it is apparent that it affected much of the Qilian Shan region.

After Mesozoic exhumation, some AFT data from the bedrock hanging wall samples and combined detrital AFT age distribution of the three Miocene samples suggest early Cenozoic cooling driven by contractional strain related to the India-Asia collision. Specifically, samples B155-1, B156-1, B157-1, B163-1 and WQL2017-170(1) from the fault-bounded Shule Nan Shan and Tuolai Nan Shan display Eocene cooling signals. Conversely, samples LB150912-2, LB150915-1 and SQL2017-216(1) from Tuolai Shan show rapid Oligocene cooling that we interpret resulted from fault-related uplift and exhumation (Fig. 8B). We note that Zuza et al. (2016b) presented a ~51 Ma apatite helium age from the Tuolai Nan Shan (Fig. 2) that is consistent with these rocks

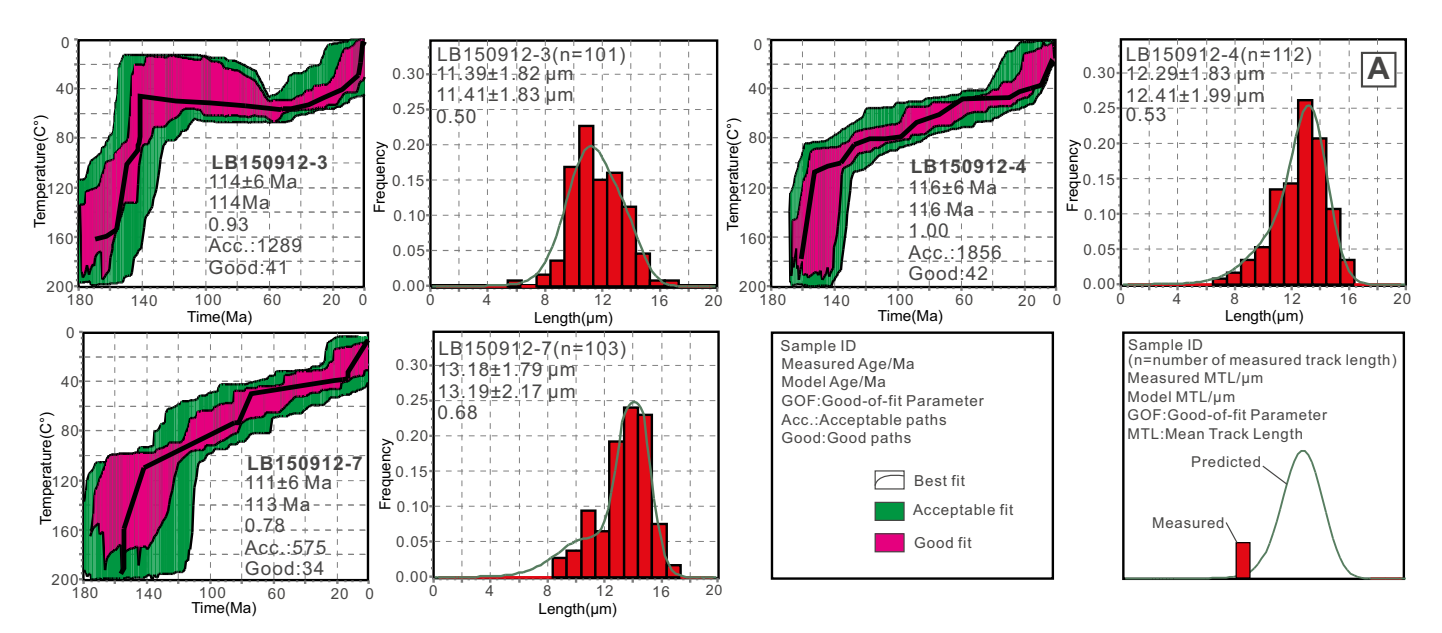


Fig. 7. AFT thermal history models and length distributions of samples from (A) footwall and (B) hanging wall of bedrock in central and northern Qilian Shan.

exhuming in the early Cenozoic. Thermal modeling of Shule Nan Shan samples suggest these rocks were exhumed to the PAZ in the early Cenozoic and have since slowly exhumed toward the surface. Combined detrital AFT age distribution of Miocene samples shows $\sim\!63$ Ma and $\sim\!50$ Ma cooling ages (Fig. 6B), which can also indicate the early Cenozoic cooling.

Cretaceous sandstone sample CQL2017-L5-2 yields an interesting thermal history (Fig. 7B) that provides important new insights for the Oilian Shan. The Cretaceous sediments in this region were deposited in an extensional setting (e.g., Chen et al., 2003, 2004, 2019b; Zuza et al., 2019) and no major post-Cretaceous deposits covered these rocks. Cretaceous strata are not thick enough (i.e., up to 1.4 km thick, Wan et al., 1989) to bury the analyzed sample to PAZ depths. Therefore the Cenozoic AFT ages and short track lengths recorded in this sample (Fig. 7B) implies that it may have been tectonically buried after Cretaceous deposition and prior to Miocene cooling. We interpret that after Cretaceous deposition, this sample was buried by early Cenozoic thrusting to PAZ depths, and was later exhumed in the Miocene. This Miocene pulse of exhumation may have eroded the rocks thrust over Cretaceous strata. There is some field evidence for Paleozoic strata thrust over Cretaceous deposits (Fig. 2). For example, field observations, geologic mapping, and seismic reflection profiles reveal early Paleozoic rocks thrust over Cretaceous strata along the North Oilan Shan, Yumu Shan, and in the Black River Valley (Fig. 2; Yang et al., 2007; Chen et al., 2019a, 2019b; Zuza et al., 2016a, 2019).

Most of the analyzed samples show cooling out of the PAZ toward the surface in middle-to-late Miocene (from ~20 Ma). This period of deformation may correspond to the reactivation of Tuolai Shan and North Qilian thrust belt, and the initiation of the western segment of Haiyuan fault (Fig. 7B). Samples LB150914-4 and WQL2017-170(1) were collected along the Haiyuan fault in the eastern part of the study area (Fig. 2). The ca. 16 Ma AFT age from sample WQL2017-170(1) probably reflects initial activity of the Haiyuan fault (Li et al., 2019; Yu et al., 2019). Although sample LB150914-4 has an older AFT age (ca. 39 Ma), its thermal modeling suggests ca. 5 Ma rapid cooling from the PAZ (Fig. 8). Yu et al. (2019) recently published a vertical AFT traverse from near our sample LB150914-4. The elevation of our sample (3128 m) fits into their lower observed PAZ, and all samples within this zone yield 40-50 Ma AFT ages and relatively short 10-12 μm track lengths. Samples from their traverse collected from higher than 3400 myielded AFT ages of ca. 17-15 Ma, which Yu et al. (2019) interpret to reflect rapid cooling associated with the initiation of the Haiyuan fault.

Therefore, our sample LB150914-4 is consistent with this interpretation and the ca. 16 Ma AFT age of sample WQL2017-170(1) also verifies the initiation timing of the Haiyuan fault.

5.2. Kinematic evolution of the Qilian Shan

Based on our new AFT ages and thermal models, we suggest three phases of cooling in the central and northern Qilian Shan during the late Jurassic-early Cretaceous, Eocene-Oligocene, and mid-late Miocene. Most publications focus on the prominent pulse of Miocene to present cooling in the Qilian Shan (George et al., 2001; Fang et al., 2003; Palumbo et al., 2009; Zheng et al., 2010, 2017; Lease et al., 2011, 2012a; Wang et al., 2011, 2016a, 2016b; Zhuang et al., 2018; Yu et al., 2019). However, statistical compilation of published thermochronology, sedimentology, and various other methods data across the entire Qilian Shan thrust belt show variable cooling ages throughout Cenozoic (Fig. 10), which represent three dominate pulses of Cenozoic deformation and exhumation history. The relatively low erosion rates and limited exhumation magnitude in northern Tibet hinder using low-temperature thermochronological methods to systematically document fault activity and cooling history.

Here, we suggest that Cretaceous and early Cenozoic tectonic events are overprinted and obscured by this obvious major pulse of Miocene reactivation. Additional evidence for this suggestion, beyond the highly variable published Cenozoic thermochronology ages (Fig. 10), includes: (1) our AFT data from Cretaceous sandstone samples which requires they were buried to PAZ depths prior to Miocene exhumation; (2) highmagnitude overthrust and nappe structures observed in the north Qilian Shan and Yumu Shan that placed early Paleozoic rocks over Cretaceous strata (Yang et al., 2007; Chen et al., 2019a; Zuza et al., 2016a, 2019). which have since been eroded; (3) kinematic modeling from strain rate data suggests that more than half of Cenozoic shortening may have occurred prior to the middle-Miocene (Zuza et al., 2019) given that India-Asia convergence rates have monotonically decelerated throughout the Cenozoic (e.g., Molnar and Stock, 2009; Copley et al., 2010; Clark, 2012); and (4) a Paleocene to early Eocene age to the Lulehe Formation (Fang et al., 2007; Yin et al., 2007a, 2008b; Ji et al., 2017; Ke et al., 2013; Lu et al., 2018; Cheng et al., 2018, 2019a, 2019b; Wu et al., 2019a, 2019b; Nie et al., 2020) with an exception of an Oligocene age to the formation (Wang et al., 2017), which is the Cenozoic basal formation in Qaidam Basin that presumably records the initiation of thrust-induced loading around the basin's periphery.

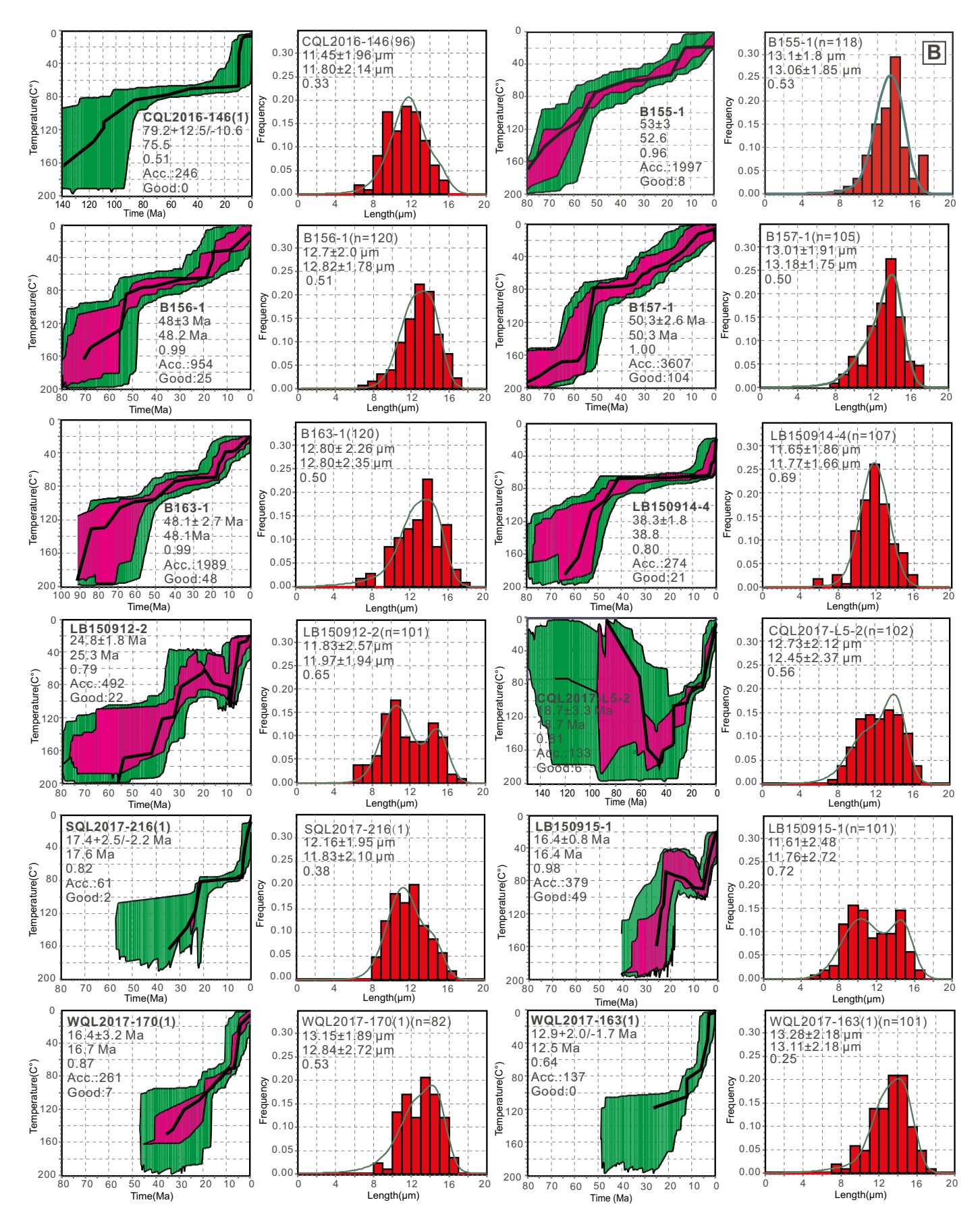


Fig. 7. (continued)

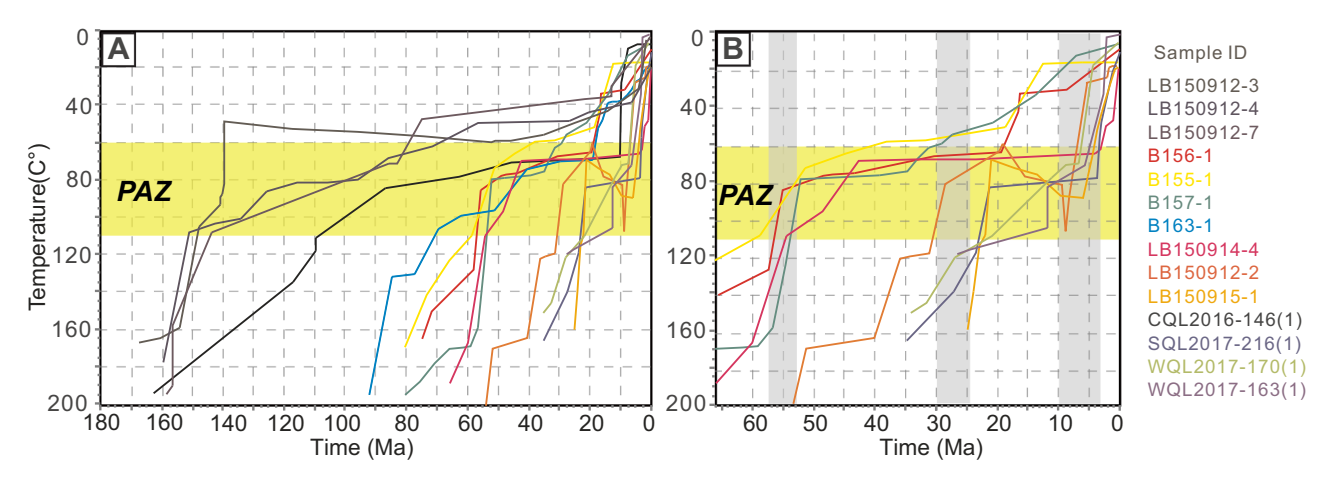


Fig. 8. Modeled inverse best fit time-temperature paths of bedrock samples show (A) Mesozoic-Present and (B) Cenozoic-Present cooling history of central and northern Qilian Shan. The yellow and grey rectangle represent the partial annealing zone of apatite and rapid cooling, respectively. (For interpretation of the references to colour in this figure legend, the reader is referred to the web version of this article.)

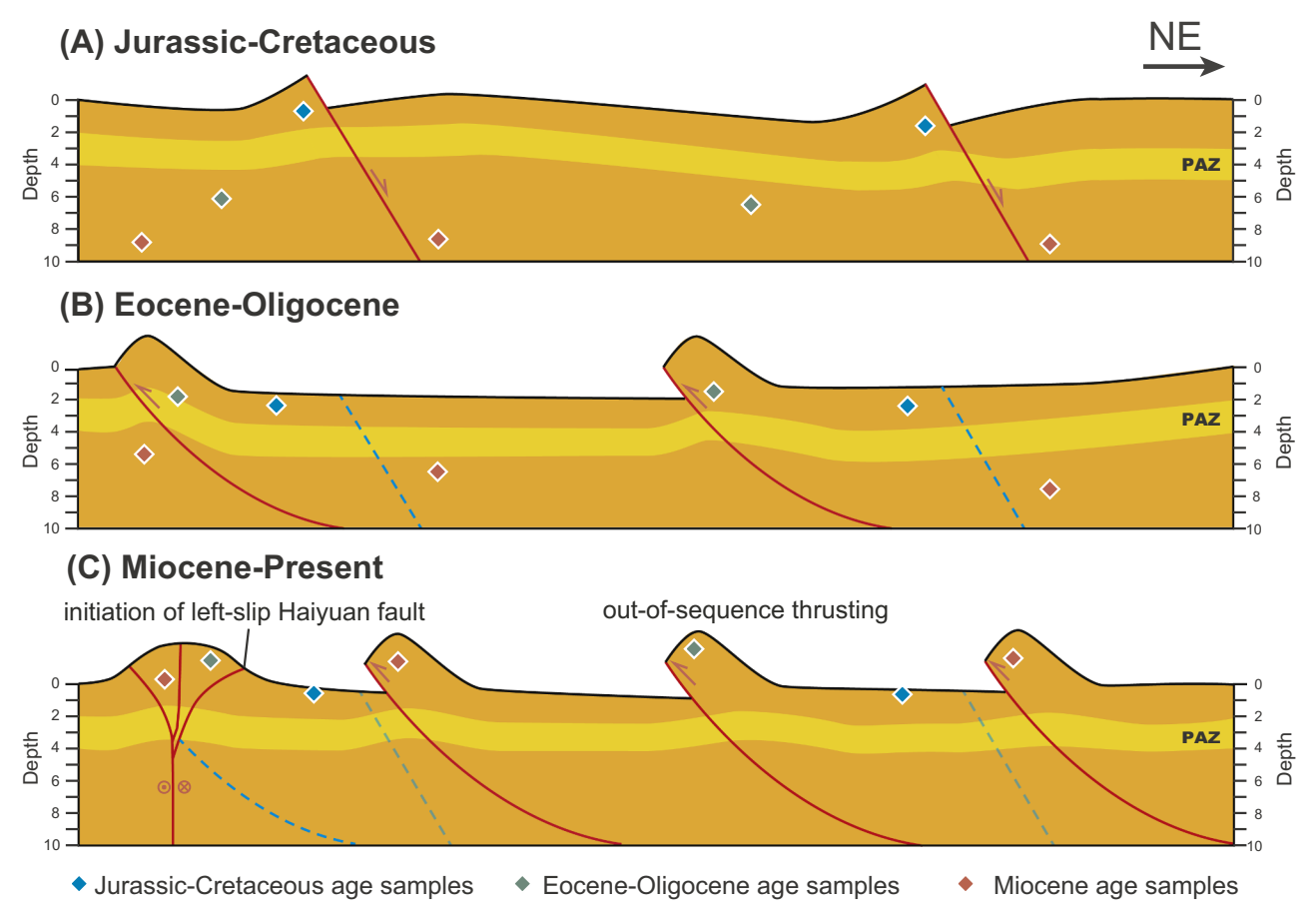


Fig. 9. Model for the Jurassic to present development in the central and northern Qilian Shan. Yellow region represents the apatite partial annealing zone (PAZ) and diamonds are example AFT samples with theoretical ages observed today. (For interpretation of the references to colour in this figure legend, the reader is referred to the web version of this article.)

Early Cenozoic deformation of Qilian Shan thrust belt initiated in the Eocene along the Qinghai Nan Shan-Zongwulong Shan in the south (Yu et al., 2017; Zuza et al., 2019) and north-dipping parallel Shule Nan Shan and Tuolai Nan Shan thrusts in the north (Fig. 2), although the extent of this deformation is not well contained because of later erosion or overprinting. Detrital samples in this study and other published datasets also record this early pulse of deformation (Fig. 6B; Jian et al., 2018; Lin et al., 2019; An et al., 2020), whereas bedrock samples are

generally affected by a Miocene cooling signature. The Miocene to present pulse of deformation is well documented by the samples from hanging wall rock bedrock in this study, and also distributed across most of the Qilian Shan (e.g., George et al., 2001; Zheng et al., 2010, 2017; Wang et al., 2011, 2016a, 2016b; Lease et al., 2012a; Yuan et al., 2013; Zhuang et al., 2018; Li et al., 2019; Yu et al., 2019) with reactivation of thrusts and initiation of left-slip Haiyuan fault.

We propose that because shortening strain appears relatively evenly

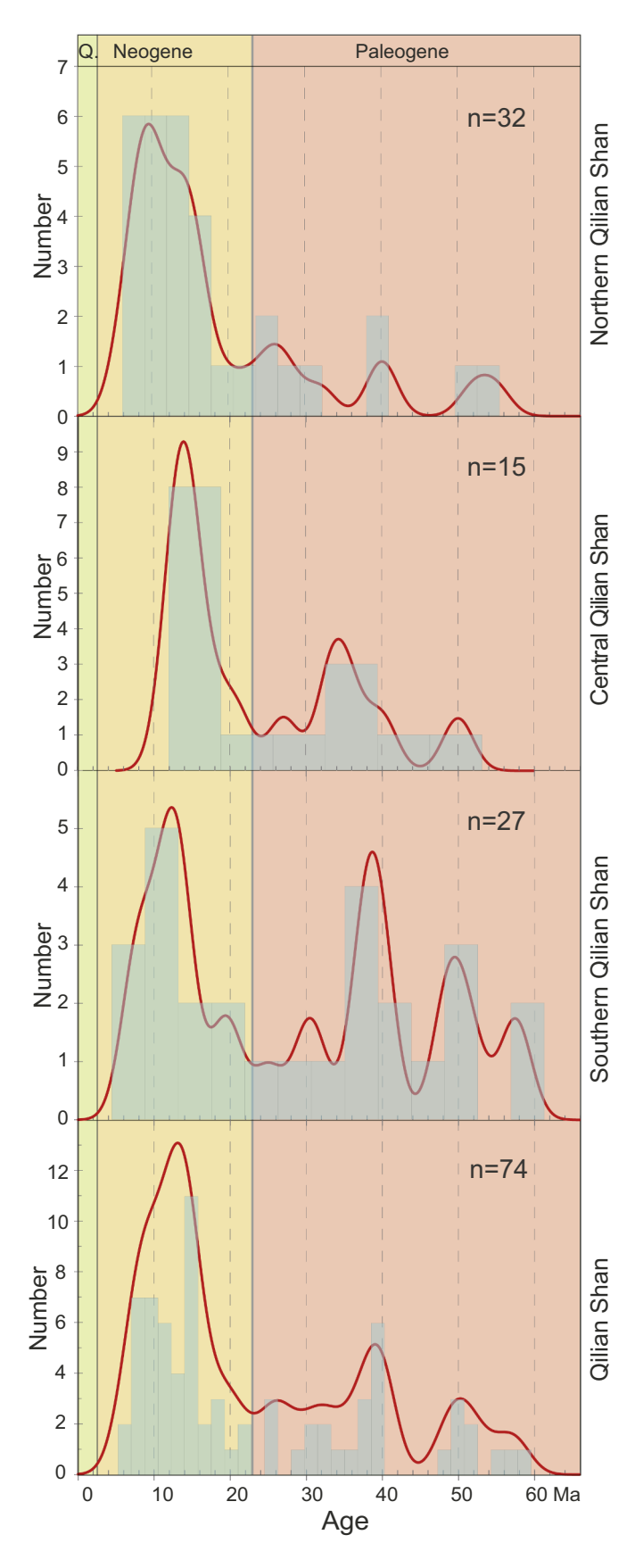


Fig. 10. Probability temporal distribution histogram of the Cenozoic tectonic events recorded in Qilian Shan, northern Tibet, as constrained by published thermochronology, sedimentology, and various other methods data (He et al., 2017a, 2017b, 2018; Cheng et al., 2016a, 2016b; Jolivet et al., 2001; Oi et al., 2013, 2015, 2016; Wan et al., 2010, 2011; Yin et al., 2002, 2008a; Wang et al., 2004; Bovet et al., 2009; Bush et al., 2016; Fang et al., 2005, 2007, 2012; Ji et al., 2017; Wei et al., 2013, Lu and Xiong, 2009; Zhuang et al., 2011, 2014; Kent-Corson et al., 2009; Yu et al., 2017; Lin et al., 2015; Zheng et al., 2010, 2017; Sun et al., 2005; Wang et al., 2003; Zhang et al., 2014; George et al., 2001; Pan et al., 2013; Dai et al., 2005; Guo et al., 2009; Liu et al., 2016; Wang et al., 2016a, 2016b, 2020; Song et al., 2001; Zhao et al., 2001; Yan et al., 2013; Yang et al., 2007; Li et al., 2019; Yu et al., 2019; Zuza et al., 2016b and this study; see Supplementary file Table S3 for compilation of Cenozoic tectonic events age datasets recorded in Qilian Shan). Abbreviation: Q.- Quaternary. Note: the number represents the amount of the data in the corresponding region. The red curve shows the normal distribution of the tectonic event ages. (For interpretation of the references to colour in this figure legend, the reader is referred to the web version of this article.)

distributed across the Qilian Shan thrust belt, as opposed to the Himalaya where strain is focused entirely on the Main Frontal Thrust (Lavé and Avouac, 2000; Zuza et al., 2019), one should expect to observe a single dominant age population in the thermochronology data across the region. Qilian Shan shortening and exhumation occurs at similar rates across strike and may be approximated by pure shear in a vertical northeast-striking cross section (Fig. 11). This predicts that most samples on the surface today should all yield a similar cooling age for a given thermochronometric system. Fig. 11 shows a schematic model for this. The dominant Miocene age (Figs. 8 and 10) only indicates that most rocks at the surface today moved through the PAZ, or comparable closure temperature window for different systems in the middle Miocene and samples that would have potentially recorded older ages have mostly been eroded away. Very few thermochronology studies reveal a paleo-PAZ (e.g., Zheng et al., 2010; Yu et al., 2019), and therefore in most cases the magnitude of exhumation remains unconstrained. Accordingly, observations of dominantly Miocene cooling may result from a sampling bias in a thrust system that is exhuming uniformly, and does not require that deformation initiated during this time. However, some sampling localities from the right structural context reveal signs of this early Cenozoic exhumation, as detailed in this study.

5.3. Implications for the Cenozoic construction of the northern Tibetan Plateau

Contemporaneous early Cenozoic deformation has been observed across most of the northern Tibetan Plateau (Jolivet et al., 2001; Clark et al., 2010; Duvall et al., 2011; Zhuang et al., 2011; Y. Wang et al., 2015; Cheng et al., 2016a, 2016b; Qi et al., 2016; Liu et al., 2017; Zhuang et al., 2018; and this study), which implies deformation started in northern Tibet shortly after the initial India-Asia collision at ~55–58 Ma (e.g., Zhu et al., 2015; Hu et al., 2015, 2016). This suggests that the early Cenozoic deformation jumped to, and reactivated the mechanically weak preexisting early Paleozoic Oilian suture zone and related structures (e.g., An et al., 2020; Bian et al., 2020) to quickly establish the northeastern boundary of the plateau that persisted throughout the Cenozoic. A relatively stationary and internal deformed northeastern boundary to the Tibetan Plateau indicates that this region must has persisted as an out-of-sequence thrust system since early Cenozoic (Fig. 9), rather than progressively propagating northward (Zheng et al., 2010, 2017; Yu et al., 2019). On a broader scale, following Eocene-Oligocene deformation along the northern boundary of the Tibetan Plateau, Miocene deformation jumped back to the Eastern Kunlun Range during the partitioning of the Paleo-Qaidam basin into the Hoh Xil and Qaidam sub-basins (Fig. 1; Wu et al., 2019a, 2019b).

This kinematic history, and early Cenozoic deformation in the

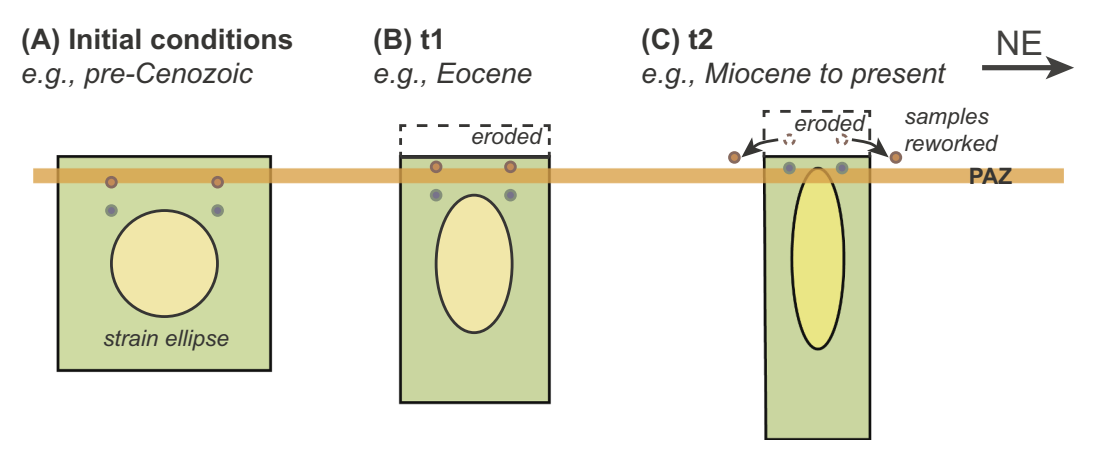


Fig. 11. Model of shortening and exhumation by pure shear in a vertical northeast-striking cross-section in the Qilian Shan. Red and green dots represent Eocene and Miocene AFT samples, respectively. (For interpretation of the references to colour in this figure legend, the reader is referred to the web version of this article.)

Qilian Shan, suggests plate-boundary stress transferred rapidly across the Himalayan-Tibetan orogen shortly after India-Asia collision. Considering restorations of Cenozoic India-Asia convergence (e.g., van Hinsbergen et al., 2011a, 2011b, van Hinsbergen, 2018; Huang et al., 2017) suggests that early Cenozoic deformation in the Oilian Shan may have initiated > 3500 km north of the India-Asia collisional front. This is at odds with the continuum deformation models (England and Houseman, 1986; Tapponnier et al., 2001) that predict a steady northward migration of deformation from the collisional front. Continuum models would favor Miocene to present growth of the Qilian Shan thrust belt, with a kinematic evolution that involved foreland propagation with successive footwall/foreland accretion. However, as outlined in this study, the Qilian Shan thrust belt did not propagate northward during the Cenozoic, but instead involved protracted out-ofsequence development. The \sim 5–10 km thick undeformed and parallel Cretaceous-Cenozoic sediments of the Hexi Corridor (e.g., Fang et al., 2005; Zhuang et al., 2011; Zuza et al., 2016a) confirm that the Hexi Corridor has remained a relatively stationary foreland to the thrust belt.

In summary, available data is consistent with the Cenozoic Qilian Shan thrust belt persisting as the stationary northern boundary of the Himalayan-Tibetan orogen and Tibetan Plateau since the early Cenozoic (e.g., Clark, 2012). It involved overprinting out-of-sequence thrusting, and the apparent dominance of Miocene cooling ages may reflect a biased artifact of relatively homogenous exhumation across the thrust system.

6. Conclusions

Geologic mapping, field observations, and AFT thermochronology provide constraints on the complex exhumation history from early Cretaceous to the present, initiation ages of thrust and strike-slip faults in the study region, and the multi-phase growth history of the northern of Tibet Plateau. Below are our primary conclusions:

- (1) The central and northern Qilian Shan experienced rapid cooling history during Cretaceous resulting from a far-field tectonic event, followed by Eocene-Oligocene thrust faulting and final accelerated cooling to the surface since ~20–10 Ma.
- (2) We suggest that the Shule Nan Shan and Tuolai Nan Shan thrust faults initiated at \sim 55 Ma, and the Tuolai Shan fault at \sim 30–25 Ma. The initiation of the western segment of the Haiyuan fault occurred at ca. 16 Ma and reactivation of the proximal Tuolai Shan has occurred since \sim 10 Ma.
- (3) The Qilian Shan thrust belt has persisted as the northern boundary of the Himalayan-Tibetan orogen and Tibetan Plateau since early Cenozoic, and underwent out-of-sequence faulting started by Eocene in accommodating the far-field compressional stress

transmitted from the early Cenozoic India-Asia collision, resulting in the multiple ranges growth and basins development in northern Tibetan Plateau.

Supplementary data to this article can be found online at https://doi.org/10.1016/j.tecto.2020.228423.

CRediT authorship contribution statement

Bing Li:Conceptualization, Investigation, Writing - original draft, Visualization.Andrew V. Zuza:Conceptualization, Investigation, Writing - review & editing, Funding acquisition.Xuanhua Chen: Investigation, Writing - review & editing, Supervision, Funding acquisition.Daogong Hu:Investigation, Writing - review & editing, Supervision.Zhaogang Shao:Investigation, Supervision, Project administration, Funding acquisition.Bangshen Qi:Investigation, Writing - review & editing.Zeng-zhen Wang:Investigation, Writing - review & editing.Drew A. Levy:Investigation, Writing - review & editing.Xiaosong Xiong:Investigation, Funding acquisition.

Declaration of competing interest

The authors declare that they have no known competing financial interests or personal relationships that could have appeared to influence the work reported in this paper.

Acknowledgments

This study is jointly supported by the geology survey projects of China Geological Survey (Nos. DD20190011 and DD20160083), the National Key Research & Development Program of China (No. 2018YFC0603701), the National Natural Science Foundation of China (No. 41774114), and the Tectonics Program of the National Science Foundation (EAR 1914501). Li gratefully thanks financial support from China Scholarship Council for funding his visit to the University of Nevada, Reno. Profound comments from Editor Prof. Z.-X. Li and reviews by Dr. Xiubin Lin and Dr. Feng Cheng greatly improved the paper. We thank Weicui Ding, Yiping Zhang, Shenglin Xu, Yongchao Wang, Yaoyao Zhang, Wei Yu, Jianjie Shi and Haohao Shao for the assistance in the field work and data processing.

References

Allen, M.B., Walters, R.J., Song, S., Saville, C., De Paola, N., Ford, J., Hu, Z., Sun, W., 2017. Partitioning of oblique convergence coupled to the fault locking behavior of fold-and-thrust belts: evidence from the Qilian Shan, northeastern Tibetan Plateau. Tectonics 36 (9), 1679–1698. https://doi.org/10.1002/2017TC004476.

- An, K., Lin, X., Wu, L., Yang, R., Chen, H., Cheng, X., Xia, Q., Zhang, F., Ding, W., Gao, S., Li, C., Zhang, Y., 2020. An immediate response to the Indian-Eurasian collision along the northeastern Tibetan Plateau: evidence from apatite fission track analysis in the Kuantan Shan-Hei Shan. Tectonophysics 774 (5), 228278. https://doi.org/10.1016/j.tecto.2019.228278.
- Bian, S., Gong, J., Chen, L., Zuza, A.V., Chen, H., Lin, X., Cheng, X., Yang, R., 2020. Diachronous uplift in intra-continental orogeny: 2D thermo-mechanical modeling of the India-Asia collision. Tectonophysics 775, 228310. https://doi.org/10.1016/j. tecto.2019.228310.
- Bovet, P.M., Ritts, B.D., Gehrels, G., Abbink, A.O., Darby, B., Hourigan, J., 2009. Evidence of Miocene crustal shortening in the North Qilian Shan from Cenozoic stratigraphy of the western Hexi Corridor, Gansu Province, China. Am. J. Sci. 309 (4), 290–329. https://doi.org/10.2475/00.4009.02.
- Burchfiel, B.C., Zhang, P., Wang, Y., Zhang, W., Song, F., Deng, Q., Molnar, P., Royden, L., 1991. Geology of the Haiyuan fault zone, Ningxia-Hui Autonomous Region, China, and its relation to the evolution of the northeastern margin of the Tibetan Plateau. Tectonics 10 (6), 1091–1110. https://doi.org/10.1029/90TC02685.
- Bush, M.A., Saylor, J.E., Horton, B.K., Nie, J., 2016. Growth of the Qaidam Basin during Cenozoic exhumation in the northern Tibetan Plateau: inferences from depositional patterns and multiproxy detrital provenance signatures. Lithosphere 8 (1), 58–82. https://doi.org/10.1130/1449.1.
- Chen, X., Yin, A., Gehrels, G.E., Cowgill, E.S., Grove, M., Harrison, T.M., Wang, X.F., 2003. Two phases of Mesozoic north-south extension in the eastern Altyn Tagh range, northern Tibetan Plateau. Tectonics 22, 1053. https://doi.org/10.1029/ 2001TC001336.
- Chen, X., Yin, A., Gehrels, G.E., Cowgill, E.S., Grove, M., Harrison, T.M., Wang, X.F., Yang, N., Liu, J., 2004. Mesozoic N-S extension in the eastern Altyn tagh range on the northern margin of the Oinghai-Tibet plateau. J. Geom. 10 (3), 193–212.
- Chen, X., Shao, Z., Xiong, X., Gao, R., Xu, S., Zhang, Y., Li, B., Wang, Y., 2019a. Early Cretaceous overthrusting of Yumu mountain and hydrocarbon prospect on the Northern margin of the Qilian orogenic belt. Acta Geoscientica Sinica (in Chinese with English abstract) 40 (3), 377–392. https://doi.org/10.3975/cagsb.2019. 050901.
- Chen, X., Shao, Z., Xiong, X., Gao, R., Liu, X., Wang, C., Li, B., Wang, Z., Zhang, Y., 2019b. Fault system, deep structure and tectonic evolution of the Qilian Orogenic Belt, Northwest China (in Chinese with English abstract). Geol. China 46 (5), 995–1020. https://doi.org/10.12029/gc20190504.
- Cheng, F., Jolivet, M., Dupont-Nivet, G., Wang, L., Yu, X., Guo, Z., 2015. Lateral extrusion along the Altyn Tagh Fault, Qilian Shan (NE Tibet): Insight from a 3D crustal budget. Terra Nova 27 (6), 416–425. https://doi.org/10.1002/2015JB012689.
- Cheng, F., Fu, S.T., Jolivet, M., Zhang, C.H., Guo, Z.J., 2016a. Source to sink relation between the Eastern Kunlun Range and the Qaidam Basin, northern Tibetan Plateau, during the Cenozoic. Geol. Soc. Am. Bull. 128 (1/2), 258–283. https://doi.org/10. 1130/B31260.1.
- Cheng, X., Lin, X., Wu, L., Chen, H., Xiao, A., Gong, J., Zhang, F., Yang, S., 2016b. The exhumation history of North Qaidam thrust belt constrained by apatite fission track thermochronology: implication for the evolution of the Tibetan Plateau. Acta Geologica Sinica (English Edition) 90 (3), 870–883. https://doi.org/10.1111/1755-6724.12730.
- Cheng, F., Garzione, C., Jolivet, M., Guo, Z., Zhang, D., Zhang, C., 2018. A new sediment accumulation model of Cenozoic depositional ages from the Qaidam basin, Tibetan Plateau. Journal of Geophysical Research: Earth Surface 123 (11), 3101–3121. https://doi.org/10.1029/2018JF004645.
- Cheng, F., Garzione, C.N., Jolivet, M., Guo, Z.T., Zhang, D.W., Zhang, C.H., Zhang, Q.Q., 2019a. Initial deformation of the northern Tibetan Plateau: insights from deposition of the Lulehe Formation in the Qaidam Basin. Tectonics 38. https://doi.org/10.1029/ 2018TC005214.
- Cheng, F., Jolivet, M., Guo, Z., Lu, H., Zhang, B., Li, X., Zhang, D., Zhang, C., Zhang, H., Wang, L., Wang, Z., 2019b. Jurassic–Early Cenozoic tectonic inversion in the Qilian Shan and Qaidam Basin, North Tibet: new insight from seismic reflection, Isopach Mapping, and Drill Core Data. Journal of Geophysical Research: Solid Earth 124 (11), 12077–12098. https://doi.org/10.1029/2019JB018086.
- Clark, M.K., 2012. Continental collision slowing due to viscous mantle lithosphere rather than topography. Nature 483 (7387), 74–77. https://doi.org/10.1038/nature10848.
- Clark, M.K., Farley, K.A., Zheng, D., Wang, Z., Duvall, A.R., 2010. Early Cenozoic faulting of the northern Tibetan Plateau margin from apatite (U-Th)/He ages. Earth Planet. Sci. Lett. 296 (1–2), 78–88. https://doi.org/10.1016/j.epsl.2010.04.051.
- Copley, A., Avouac, J.P., Royer, J.Y., 2010. India-Asia collision and the Cenozoic slow-down of the Indian plate: implications for the forces driving plate motions. Journal of Geophysical Research–Solid Earth 115 (B3), B03410. https://doi.org/10.1029/2009.JB006634.
- Cowgill, E., Yin, A., Harrison, T.M., Wang, X.F., 2003. Reconstruction of the Altyn Tagh fault based on U-Pb geochronology: role of back thrusts, mantle sutures, and heterogeneous crustal strength in forming the Tibetan Plateau. Journal of Geophysical Research-Solid Earth 108 (B7), 2346. https://doi.org/10.1029/2002JB002080.
- Craddock, W., Kirby, E., Zhang, H., 2011. Late Miocene-Pliocene range growth in the interior of the northeastern Tibetan Plateau. Lithosphere 3 (6), 420–438. https://doi. org/10.1130/L159.1.
- Craddock, W.H., Kirby, E., Zhang, H., Clark, M.K., Champagnac, J.D., Yuan, D., 2014.
 Rates and style of Cenozoic deformation around the Gonghe Basin, northeastern
 Tibetan Plateau. Geosphere 10 (6), 1255–1282. https://doi.org/10.1130/GES01024.1.
- Cui, Z., Gao, Q., Liu, G., 1997. The initial elevation of palaeo-karst and planation surfaces on Tibet Plateau. Chin. Sci. Bull. 43 (11), 934–939. https://doi.org/10.1007/ BF02882552.
- Curry, M.A.E., Barnes, J.B., Colgan, J.P., 2016. Testing fault growth models with low-

- temperature thermochronology in the northwest Basin and Range, USA. Tectonics 35 (10), 2467–2492. https://doi.org/10.1002/2016TC004211.
- Dai, S., Fang, X., Song, C., Junping, G., Donglin, G., Li, J., 2005. Early tectonic uplift of the northern Tibetan Plateau. Chinese Science Bulletin (in Chinese with English abstract) 50, 1642–1652. https://doi.org/10.1360/03wd0255.
- Dai, S., Fang, X., Dupont-Nivet, G., Song, C., Gao, J., Krijgsman, W., Langereis, C., Zhang, W., 2006. Magnetostratigraphy of Cenozoic sediments from the Xining Basin: tectonic implications for the northeastern Tibetan Plateau. Journal of Geophysical Research-Solid Earth 111, B11102. https://doi.org/10.1029/2005JB004187.
- Dodson, M.H., 1973. Closure temperature in cooling geochronological and petrological systems. Contrib. Mineral. Petrol. 40, 259–274. https://doi.org/10.1007/
- Dupont-Nivet, G., Horton, B.K., Butler, R.F., Wang, J., Zhou, J., Waanders, G.L., 2004. Paleogene clockwise tectonic rotation of the Xining-Lanzhou region, northeastern Tibetan Plateau. Journal of Geophysical Research-Solid Earth 109, B04401. https://doi.org/10.1029/2003JB002620.
- Duvall, A.R., Clark, M.K., van der Pluijm, B.A., Li, C., 2011. Direct dating of Eocene reverse faulting in northeastern Tibet using Ar-dating of fault clays and low-temperature thermochronometry. Earth Planet. Sci. Lett. 304 (3–4), 520–526. https:// doi.org/10.1016/j.epsl.2011.02.028.
- Duvall, A.R., Clark, M.K., Kirby, E., Farley, K.A., Craddock, W.H., Li, C., Yuan, D.Y., 2013. Low-temperature thermochronometry along the Kunlun and Haiyuan faults, NE Tibetan Plateau: evidence for kinematic change during late-stage orogenesis. Tectonics 32 (5), 1190–1211. https://doi.org/10.1002/tect.20072.
- England, P., Houseman, G., 1986. Finite strain calculations of continental deformation: 2. Comparison with the India-Asia collision zone. Journal of Geophysical Research-Solid Earth 91 (B3), 3664–3676. https://doi.org/10.1029/JB091iB03p03664.
- Fang, X., Garzione, C., Van der Voo, R., Li, J., Fan, M., 2003. Flexural subsidence by 29 Ma on the NE edge of Tibet from the magnetostratigraphy of Linxia Basin, China. Earth Planet. Sci. Lett. 210 (3–4), 545–560. https://doi.org/10.1016/S0012-821X (03)0014-0.
- Fang, X., Zhao, Z., Li, J., Yan, M., Pan, B., Song, C., Dai, S., 2005. Magnetostratigraphy of the late Cenozoic Laojunmiao anticline in the northern Qilian Mountains and its implications for the northern Tibetan Plateau uplift. Sci. Science in China Series D-Earth Sciences 48 (7), 1040–1051. https://doi.org/10.5483/BMBRep.2008.41.5.353.
- Fang, X., Zhang, W., Meng, Q., Gao, J., Wang, X., King, J., Song, C., Dai, S., Miao, Y., 2007. High-resolution magnetostratigraphy of the Neogene Huaitoutala section in the eastern Qaidam Basin on the NE Tibetan Plateau, Qinghai Province, China and its implication on tectonic uplift of the NE Tibetan Plateau. Earth Planet. Sci. Lett. 258 (1–2), 293–306. https://doi.org/10.1016/j.epsl.2007.03.042.
- Fang, X., Liu, D., Song, C., Dai, S., Meng, Q., 2012. Oligocene slow and Miocene-Quaternary rapid deformation and uplift of the Yumu Shan and North Qilian Shan: evidence from high-resolution magnetostratigraphy and tectonosedimentology. In: Jovane, L., Herrero-Bervera, E., Hinnov, L.A., Housen, B. (Eds.), Magnetic Methods and the Timing of Geological Processes. 373. Geological Society, London, Special Publication, pp. 149–171.
- Flowers, R.M., Farley, K.A., Ketcham, R.A., 2015. A reporting protocol for thermochronologic modeling illustrated with data from the Grand Canyon. Earth Planet. Sci. Lett. 432, 425–435 (doi003A10.1016/j.epsl.2015.09.053).
- Galbraith, R.F., 1981. On statistical models for fission track counts. J. Int. Assoc. Math. Geol. 13 (6), 471–478. https://doi.org/10.1007/BF01034498.
- Galbraith, R.F., Green, P.F., 1990. Estimating the component ages in a finite mixture. International Journal of Radiation Applications and Instrumentation. Part D. Nuclear Tracks and Radiation Measurements 17 (3), 197–206. https://doi.org/10.1016/ 1359-0189(90)0035-V
- Galbraith, R.F., Laslett, G.M., 1993. Statistical models for mixed fission track ages. Nuclear Tracks and Radiation Measurements 21, 459–470. https://doi.org/10.1016/ 1359-0189(93)90185-C.
- Gallagher, K., Brown, R., Johnson, C., 1998. Fission track analysis and its applications to geological problems. Annual Reviews of Earth & Planetary Science 26, 519–572. https://doi.org/10.1146/annurev.earth.26.1.519.
- Gehrels, G.E., Yin, A., Wang, X.F., 2003a. Detrital zircon geochronology of the northeastern Tibetan Plateau. Geol. Soc. Am. Bull. 115 (7), 881–896. https://doi.org/10.1130/0016-7606 (2003)115 < 0881:DGOTNT > 2.0.CO;2.
- Gehrels, G.E., Yin, A., Wang, X.F., 2003b. Magmatic history of the Altyn Tagh, Nan Shan, and Qilian Shan region of western China. Journal of Geophysical Research-Solid Earth 108 (B9), 2423. https://doi.org/10.1029/2002JB001876.
- George, A.D., Marshallsea, S.J., Wyrwoll, K.H., Jie, C., Yanchou, L., 2001. Miocene cooling in the northern Qilian Shan, northeastern margin of the Tibetan Plateau, revealed by apatite fission-track and vitrinite-reflectance analysis. Geology 29 (10), 939–942. https://doi.org/10.1130/0091-7613(2001)029 < 0939:MCITNQ > 2.0. CO:2.
- Gleadow, A.J.W., 1981. Fission-track dating methods: what are the real alternatives? Nuclear Tracks 5 (1–2), 3–14. https://doi.org/10.1016/0191-278X(81)90021-4.
- Gleadow, A.J.W., Brown, R.W., 2000. Fission track thermochronology and the long-term denudational response to tectonics. In: Summerfield, M.A. (Ed.), Geomorphology and Global Tectonics. John Wiley, New York, pp. 57–75.
- Gleadow, A.J.W., Duddy, I.R., 1981. A natural long-term track annealing experiment for apatite. Nuclear Tracks 5 (1–2), 169–174. https://doi.org/10.1016/0191-278X(81) 90039-1.
- Gleadow, A.J.W., Duddy, I.R., Green, P.F., Lovering, J.F., 1986. Confined fission track lengths in apatite: a diagnostic tool for thermal history analysis. Contrib. Mineral. Petrol. 94 (4), 405–415. https://doi.org/10.1007/BF00376334.
- Green, P.F., 1981. A new look at statistics in fission-track dating. Nuclear tracks 5 (1–2), 77–86. https://doi.org/10.1016/0191-278X(81)90029-9.
- Green, P.F., 1988. The relationship between track shortening and fission track age

reduction in apatite: combined influences of inherent instability, annealing anisotropy, length bias and system calibration. Earth Planet. Sci. Lett. 89 (3–4), 335–352. https://doi.org/10.1016/0012-821X(88)90121-5.

- Green, P.F., Duddy, I.R., Gleadow, A.J.W., Tingate, P.R., Laslett, G.M., 1986. Thermal annealing of fission tracks in apatite: 1. A qualitative description. Chemical Geology: Isotope Geoscience section 59, 237–253. https://doi.org/10.1016/0168-9622(86) 20074.6
- Guo, Z., Lu, J., Zhang, Z., 2009. Cenozoic exhumation and thrusting in the Northern Qilian Shan, Northeastern margin of the Tibetan Plateau: constraints from sedimentological and apatite fission-track data. Acta Geologica Sinica (English Edition) 83 (3), 562–579. https://doi.org/10.1111/j.1755-6724.2009.00045.x.
- Guo, R., Li, S., Yu, S., Dai, L., Liu, Y., Peng, Y., Zhou, Z., Wang, Y., Liu, Y., Wang, Q., 2019. Collisional processes between the Qiangtang Block and the Lhasa Block: Insights from structural analysis of the Bangong-Nujiang Suture Zone, Central Tibet. Geol. J. 54 (2), 946–960. https://doi.org/10.1002/gj.3420.
- He, S., Wang, H., Chen, J., Xu, X., Zhang, H., Ren, G., Yu, J., 2007. LA-ICP-MS U-Pb zircon geochronology of basic dikes within Maxianshan rock group in the central Qilian orogenic belt and its tectonic implications. J. China Univ. Geosci. 18 (1), 19–29. https://doi.org/10.1016/S1002-0705(07)60015-6.
- He, P., Song, C., Wang, Y., Chen, L., Chang, P., Wang, Q., Ren, B., 2017a. Cenozoic exhumation in the Qilian Shan, northeastern Tibetan Plateau: evidence from detrital fission track thermochronology in the Jiuquan Basin. Journal of Geophysical Research: Solid Earth 122 (8), 6910–6927. https://doi.org/10.1002/2017jb014216.
- He, P., Wang, X., Song, C., Wang, Q., Deng, L., Zhong, S., 2017b. Cenozoic evolution of the Western Qinling Mt. Range based on thermochronologic and sedimentary records from the Wudu Basin, NE Tibetan Plateau. J. Asian Earth Sci. 138, 484–494. https:// doi.org/10.1016/j.jseaes.2017.02.033.
- He, P., Song, C., Wang, Y., Meng, Q., Chen, L., Yao, L., Huang, S., Feng, W., Chen, S., 2018. Cenozoic deformation history of the Qilian Shan (northeastern Tibetan Plateau) constrained by detrital apatite fission-track thermochronology in the northeastern Qaidam Basin. Tectonophysics 749 (6), 1–11. https://doi.org/10.1016/j.tecto.2018.10.017.
- He, C., Zhang, Y., Li, J., Li, H., Sun, D., Xiong, J., 2019. Kinematics of the Maxian Mountain Fault, Northeastern Tibetan Plateau: the history of Cretaceous-Cenozoic Sedimentary and Tectonic Deformation. Acta Geoscientica Sinica (In Chinese with English abstract) 40 (4), 563–587. https://doi.org/10.3975/cagsb.2018.111901.
- van Hinsbergen, D.J., 2018. Reconciling Contradictions in Kinematic Reconstructions of Greater India and Tibet, and the Geodynamics of Plateau Rise and Plate Motion Change: Indianapolis, Indiana, the Geological Society of America Annual Meeting, Abstract 287–8.
- van Hinsbergen, D.J., Kapp, P., Dupont-Nivet, G., Lippert, P.C., DeCelles, P.G., Torsvik, T.H., 2011a. Restoration of Cenozoic deformation in Asia and the size of Greater India. Tectonics 30 (5), TC5003. https://doi.org/10.1029/2011TC002908.
- van Hinsbergen, D.J., Steinberger, B., Doubrovine, P.V., Gassmöller, R., 2011b.

 Acceleration and deceleration of India-Asia convergence since the Cretaceous: roles of mantle plumes and continental collision. Journal of Geophysical Research–Solid Earth 116 (B6), B06101. https://doi.org/10.1029/2010JB008051.
- Hough, B.G., Garzione, C.N., Wang, Z., Lease, R.O., Burbank, D.W., Yuan, D., 2011. Stable isotope evidence for topographic growth and basin segmentation: implications for the evolution of the NE Tibetan Plateau. Geol. Soc. Am. Bull. 123 (1–2), 168–185. https://doi.org/10.1130/B30090.1.
- Hu, N.G., Xu, A.D., Yang, J.X., 2005. Characteristics and tectonic environment of Zhigoumen pluton in Longshoushan area. J. Earth Sci. Environ. 27, 5–11. https://doi. org/10.3969/j.issn.1672-6561.2005.02.002. (in Chinese with English abstract).
- Hu, X., Garzanti, E., Moore, T., Raffi, I., 2015. Direct stratigraphic dating of India-Asia collision onset at the Selandian (middle Paleocene, 59 ± 1 Ma). Geology 43 (10), 859–862. https://doi.org/10.1130/G36872.1.
- Hu, X., Garzanti, E., Wang, J., Huang, W., An, W., Webb, A., 2016. The timing of India-Asia collision onset—facts, theories, controversies. Earth Sci. Rev. 160, 264–299. https://doi.org/10.1016/j.earscirev.2016.07.014.
- Huang, W., Lippert, P.C., Jackson, M.J., Dekkers, M.J., Zhang, Y., Li, J., Guo, Z., Kapp, P., van Hinsbergen, D.J., 2017. Remagnetization of the Paleogene Tibetan Himalayan carbonate rocks in the Gamba area: Implications for reconstructing the lower plate in the India-Asia collision. J. Geophys. Res. Solid Earth 122 (2), 808–825. https://doi.org/10.1002/2016JB013662.
- Hurford, A.J., 1990. Standardization of fission track dating calibration: recommendation by the Fission Track Working Group of the IUGS subcommission on geochronology. Chemical Geology: Isotope Geoscience section 80 (2), 171–178. https://doi.org/10. 1016/0168-9622(90)90025-8.
- Ji, J., Zhang, K., Clift, P.D., Zhuang, G., Song, B., Ke, X., Xu, Y., 2017. High-resolution magnetostratigraphic study of the Paleogene-Neogene strata in the Northern Qaidam Basin: implications for the growth of the Northeastern Tibetan Plateau. Gondwana Res. 46, 141–155. https://doi.org/10.1016/j.gr.2017.02.015.
- Jia, L., Wang, C., Shen, Y., Hu, D., Zhao, X., Qi, B., Zhang, Y., Tao, T., 2018. Formation age of the planation surface in Qilian Mountains: evidence from the electron spin resonance (ESR) dating. Quaternary Sciences 38 (3), 668–679. https://doi.org/10.11928/j.issn.1001-7410.2018.03.11. (In Chinese with English abstract).
- Jian, X., Guan, P., Zhang, W., Liang, H., Feng, F., Fu, L., 2018. Late Cretaceous to early Eocene deformation in the northern Tibetan Plateau: Detrital apatite fission track evidence from northern Qaidam basin. Gondwana Res. 60, 94–104. https://doi.org/ 10.1016/j.gr.2018.04.007.
- Jiang, R.B., Chen, X.H., Dang, Y.Q., Yin, A., Wang, L.Q., Jiang, W.M., Wan, J.L., Li, L., Wang, X.F., 2008. Apatite fission track evidence for two phases Mesozoic–Cenozoic thrust faulting in eastern Qaidam Basin. Chin. J. Geophys. 51 (1), 116–124. https://doi.org/10.3321/j.issn:0001–5733.2008.01.015.
- Jolivet, M., Brunel, M., Seward, D., Xu, Z., Yang, J., Roger, F., Tapponnier, P., Malavieille,

- J., Arnaud, N., Wu, C., 2001. Mesozoic and Cenozoic tectonics of the northern edge of the Tibetan Plateau: fission-track constraints. Tectonophysics 343 (1–2), 111–134. https://doi.org/10.1016/S0040-1951(01)00196-2.
- Kapp, P., DeCelles, P.G., Gehrels, G.E., Heizler, M., Ding, L., 2007. Geological records of the Lhasa-Qiangtang and Indo-Asian collisions in the Nima area of central Tibet. Geol. Soc. Am. Bull. 119 (7–8), 917–932. https://doi.org/10.1130/B26033.1.
- Ke, X., Ji, J., Zhang, K., Kou, X., Song, B., Wang, C., 2013. Magnetostratigraphy and anisotropy of magnetic susceptibility of the Lulehe Formation in the northeastern Qaidam Basin. Acta Geologica Sinica-English Edition 87 (2), 576–587. https://doi. org/10.1111/1755-6724.12069.
- Kent-Corson, M.L., Ritts, B.D., Zhuang, G., Bovet, P.M., Graham, S.A., Page Chamberlain, C., 2009. Stable isotopic constraints on the tectonic, topographic, and climatic evolution of the northern margin of the Tibetan Plateau. Earth and Planetary Sciences Letters 282 (1–4), 158–166. https://doi.org/10.1016/j.epsl.2009.03.011.
- Ketcham, R.A., 2005. Forward and inverse modeling of low-temperature thermochronometry data. Rev. Mineral. Geochem. 58 (1), 275–314. https://doi.org/10. 2138/rmg.2005.58.11.
- Ketcham, R.A., Carter, A., Donelick, R.A., Barbarand, J., Hurford, A.J., 2007. Improved modeling of fission-track annealing in apatite. The American Mineralogist 92 (5–6), 799–810. https://doi.org/10.2138/am.2007.2281.
- Lavé, J., Avouac, J.P., 2000. Active folding of fluvial terraces across the Siwaliks Hills, Himalayas of central Nepal. Journal of Geophysical Research-Solid Earth 105 (B3), 5735–5770. https://doi.org/10.1029/1999JB900292.
- Lease, R.O., Burbank, D.W., Gehrels, G.E., Wang, Z., Yuan, D., 2007. Signatures of mountain building: detrital zircon U/Pb ages from northeastern Tibet. Geology 35, 239–242. https://doi.org/10.1130/G23057A.1.
- Lease, R.O., Burbank, D.W., Clark, M.K., Farley, K.A., Zheng, D., Zhang, H., 2011. Middle Miocene reorganization of deformation along the northeastern Tibetan Plateau. Geology 39 (4), 359–362. https://doi.org/10.1130/G31356.1.
- Lease, R.O., Burbank, D.W., Hough, B., Wang, Z., Yuan, D., 2012a. Pulsed Miocene range growth in northeastern Tibet: insights from Xunhua Basin magnetostratigraphy and provenance. Geol. Soc. Am. Bull. 124 (5–6), 657–677. https://doi.org/10.1130/ B30524.1.
- Lease, R.O., Burbank, D.W., Zhang, H., Liu, J., Yuan, D., 2012b. Cenozoic shortening budget for the northeastern edge of the Tibetan Plateau: is lower crustal flow necessary? Tectonics 31 (3), TC3011. https://doi.org/10.1029/2011TC003066.
- Li, J.J., Fang, X.M., 1999. Uplift of the Tibetan Plateau and environmental changes. Chin. Sci. Bull. 44 (23), 2117–2124. https://doi.org/10.1007/BF03182692.
- Li, B., Chen, X., Zuza, A.V., Hu, D., Ding, W., Huang, P., Xu, S., 2019. Genozoic cooling history of the North Qilian Shan, northern Tibetan Plateau, and the initiation of the Haiyuan fault: Constraints from apatite- and zircon-fission track thermochronology. Tectonophysics 751, 101–124. https://doi.org/10.1016/j.tecto.2018.12.005.
- Tectonophysics 751, 101–124. https://doi.org/10.1016/j.tecto.2018.12.005. Lin, X., Chen, H., Wyrwoll, K.H., Batt, G.E., Liao, L., Xiao, J., 2011. The uplift history of the Haiyuan-Liupan Shan region northeast of the present Tibetan Plateau: Integrated constraint from stratigraphy and thermochronology. The Journal of Geology 119 (4), 372–393. https://doi.org/10.1086/660190.
- Lin, X., Zheng, D., Sun, J., Windley, B.F., Tian, Z., Gong, Z., Jia, Y., 2015. Detrital apatite fission track evidence for provenance change in the Subei Basin and implications for the tectonic uplift of the Danghe Nan Shan (NW China) since the mid-Miocene. J. Asian Farth Sci. 111, 302–311. https://doi.org/10.1016/j.iseaes.2015.07.007
- Asian Earth Sci. 111, 302–311. https://doi.org/10.1016/j.jseaes.2015.07.007. Lin, X., Wyrwoll, K.H., Chen, H., Cheng, X., 2016. On the timing and forcing mechanism of a mid-Miocene arid climate transition at the NE margins of the Tibetan Plateau: stratigraphic and sedimentologic evidence from the Sikouzi Section. Int. J. Earth Sci. 105 (3), 1039–1049. https://doi.org/10.1007/s00531-015-1213-z.
- Lin, X., Tin, Y., Donelick, R., Liu-Zeng, J., Cleber, S., Li, C., Wu, Q., Li, Z., 2019. Mesozoic and Cenozoic tectonics of the northeastern edge of the Tibetan plateau: evidence from modern river detrital apatite fission-track age constraints. J. Asian Earth Sci. 170, 84–95. https://doi.org/10.1016/j.jseaes.2018.10.028.
- Liu, Y.J., Neubauer, F., Genser, J., Takasu, A., Ge, X.H., Handler, R., 2006. ⁴⁰Ar/³⁹Ar ages of blueschist facies pelitic schists from Qingshuigou in the Northern Qilian Mountains, western China. Island Arc 15 (1), 187–198. https://doi.org/10.1111/j. 1440-1738.2006.00508.x.
- Liu, C., Wang, W., Zhang, P., Pang, J., Yu, J., 2016. Magnetostratigraphy and magnetic anisotropy of the Neogene sediments in the Qilian Basin. Chinese Journal of Geophysics (in Chinese with English abstract) 59 (8), 2965–2978. https://doi.org/10. 6038/cjg20160820.
- Liu, D., Li, H., Sun, Z., Pan, J., Wang, M., Wang, H., 2017. AFT dating constrains the Cenozoic uplift of the Qimen Tagh Mountains, Northeast Tibetan Plateau, comparison with LA-ICPMS Zircon U-Pb ages. Gondwana Res. 41, 438–450. https://doi.org/10. 1016/j.gr.2015.10.008.
- Lu, H., Xiong, S., 2009. Magnetostratigraphy of the Dahonggou section, northern Qaidam Basin and its bearing on Cenozoic tectonic evolution of the Qilian Shan and Altyn Tagh Fault. Earth Planet. Sci. Lett. 288 (3–4), 539–550. https://doi.org/10.1016/j. epsl. 2009.10.016.
- Lu, H.J., Ye, J.C., Guo, L.C., Pan, J.W., Xiong, S.F., Li, H.B., 2018. Towards a clarification of the provenance of Cenozoic sediments in the northern Qaidam Basin. Lithosphere 11 (2), 252–272. https://doi.org/10.1130/L1037.1.
- McDannell, K.T., Issler, D.R., O'Sullivan, P.B., 2019. Radiation-enhanced fission track annealing revisited and consequences for apatite thermochronometry. Geochim. Cosmochim. Acta 252, 213–239.
- Meyer, B., Tapponnier, P., Bourjot, L., Metivier, F., Gaudemer, Y., Peltzer, G., Shunmin, G., Zhitai, C., 1998. Crustal thickening in Gansu-Qinghai, lithospheric mantle subduction, and oblique, strike-slip controlled growth of the Tibet plateau. Geophys. J. Int. 135 (1), 1–47. https://doi.org/10.1046/j.1365-246X.1998.00567.x.
- Molnar, P., Stock, J.M., 2009. Slowing of India's convergence with Eurasia since 20 Ma and its implications for Tibetan mantle dynamics. Tectonics 28 (3), TC3001. https://

- doi.org/10.1029/2008TC002271.
- Molnar, P., England, P., Martinod, J., 1993. Mantle dynamics, uplift of the Tibetan Plateau, and the Indian monsoon. Rev. Geophys. 31 (4), 357–396. https://doi.org/10. 1029/93RG02030.
- Molnar, P., Boos, W.R., Battisti, D.S., 2010. Orographic controls on climate and paleoclimate of Asia: thermal and mechanical roles for the Tibetan Plateau. Annual Reviews of Earth & Planetary Science 38, 77–102. https://doi.org/10.1146/annurevearth-040809-152456.
- Nie, J., Ren, X., Saylor, J.E., Su, Q., Horton, B.K., Bush, M.A., Chen, W., Pfaff, K., 2020. Magnetic polarity stratigraphy, provenance, and paleoclimate analysis of Cenozoic strata in the Qaidam Basin, NE Tibetan Plateau. Geol. Soc. Am. Bull. 132 (1–2), 310–320. https://doi.org/10.1130/B35175.1.
- O'Sullivan, P.B., Parrish, R.R., 1995. The importance of apatite composition and single-grain ages when interpreting fission track data from plutonic rocks: a case study from the Coast Ranges, British Columbia. Earth Planet. Sci. Lett. 132 (1–4), 213–224. https://doi.org/10.1016/0012-821X(95)00058-K.
- Palumbo, L., Hetzel, R., Tao, M., Li, X., Guo, J., 2009. Deciphering the rate of mountain growth during topographic presteady state: an example from the NE margin of the Tibetan Plateau. Tectonics 28 (4), TC4017. https://doi.org/10.1029/2009TC002455.
- Pan, B., Li, Q., Hu, F., Geng, H., Liu, Z., Jiang, S., Yuan, W., 2013. Cretaceous and Cenozoic cooling history of the eastern Qilian Shan, north-eastern margin of the Tibetan Plateau: evidence from apatite fission-track analysis. Terra Nova 25 (6), 431–438. https://doi.org/10.1111/ter.12052.
- Pullen, A., Kapp, P., Gehrels, G.E., Vervoort, J.D., Ding, L., 2008. Triassic continental subduction in Central Tibet and Mediterranean-style closure of the Paleo-Tethys Ocean. Geology 36 (5), 351–354. https://doi.org/10.1130/G24435A.1.
- Qi, B., Hu, D., Wang, J., Wang, X., Zhang, X., Zhang, Y., Yang, X., Gao, X., 2013. ESR dating of the Palaeogene in Muli Basin in the middle of Qilian Mountains and its geological significance. Journal of Geomechanics (In Chinese with English abstract) 19 (4), 392–402.
- Qi, B., Hu, D., Yang, X., Zhang, X., Zhao, X., 2015. Paleoelevation of the Qilian Mountain Inferred from Carbon and Oxygen Isotopes of Cenozoic Strata. Acta Geoscientica Sinica (In Chinese with English abstract) 36 (3), 323–332. https://doi.org/10.3975/ cassb.2015.03.07.
- Qi, B., Hu, D., Yang, X., Zhang, Y., Tan, C., Zhang, P., Feng, C., 2016. Apatite fission track evidence for the Cretaceous-Cenozoic cooling history of the Qilian Shan (NW China) and for stepwise northeastward growth of the northeastern Tibetan Plateau since early Eocene. J. Asian Earth Sci. 124, 28–41. https://doi.org/10.1016/j.jseaes.2016. 04.009.
- Raymo, M.W., Ruddiman, W.F., 1992. Tectonic forcing of late Cenozoic climate. Nature 359, 117–122. https://doi.org/10.1130/0016-7606 (2000)112 < 1091:UHOTCA > 2. 0.CO:2.
- Ritts, B.D., Biffi, U., 2000. Magnitude of post-Middle Jurassic (Bajocian) displacement on the central Altyn Tagh fault system, northwest China. Geol. Soc. Am. Bull. 112 (1), 61–74. https://doi.org/10.1130/0016-7606 (2000)112 < 61:MOPJBD > 2.0.CO;2.
- Royden, L.H., Clark, B., van der Hilst, R.D., 2008. The geological evolution of the Tibetan Plateau. Science 321 (5892), 1054–1058. https://doi.org/10.1126/science.1155371.
- Sobel, E.R., Chen, J., Heermance, R.V., 2006a. Late Oligocene Early Miocene initiation of shortening in the Southwestern Chinese Tian Shan: implications for Neogene shortening rate variations. Earth Planet. Sci. Lett. 247, 70–81. https://doi.org/10.1016/j.epsl.2006.03.048.
- Sobel, E.R., Oskin, M., Burbank, D., Miskolaichuk, A., 2006b. Exhumation of base-mentcored uplifts: example of the Kyrgyz range quantified with apatite fission track thermochronology. Tectonics 25 (2), TC2008. https://doi.org/10.1029/2005TC001809.
- Song, C., Fang, X., Li, J., Gao, J., Zhao, Z., Fan, M., 2001. Tectonic uplift and sedimentary evolution of the Jiuxi Basin in the northern margin of the Tibetan Plateau since 13 Ma BP. Sci. China Ser. D Earth Sci. 44 (s1), 192–202. https://doi.org/10.1007/ bf0/2011087
- Song, S., Niu, Y., Su, L., Xia, X., 2013. Tectonics of the North Qilian orogen, NW China. Gondwana Res. 23 (4), 1378–1401. https://doi.org/10.1016/j.gr.2012.02.004.
- Song, S., Yang, L., Zhang, Y., Niu, Y., Wang, C., Su, L., Gao, Y., 2017. Qi-Qin Accretionary Belt in Central China Orogen: accretion by trench jam of oceanic plateau and formation of intra-oceanic arc in the Early Paleozoic Qin-Qi-Kun Ocean. Science Bulletin 62 (15), 1035–1098. https://doi.org/10.1016/j.scib.2017.07.009.
- Song, S., Wu, Z., Yang, L., Su, L., Xia, X., Wang, C., Dong, J., Zhou, C., Bi, H., 2019. Ophiolite belts and evolution of the Proto-Tethys Ocean in the Qilian Orogen. Acta Petrologica Sinica (in Chinese with English abstract) 35 (10), 2948–2970. 2948-2970. 10.18654/1000-0569/2019.10.02.
- Spurlin, M.S., Yin, A., Horton, B.K., Zhou, J., Wang, J., 2005. Structural evolution of the Yushu-Nangqian region and its relationship to syn-collisional igneous activity eastcentral Tibet. Geol. Soc. Am. Bull. 117 (9–10), 1293–1317. https://doi.org/10.1130/ R25572.1
- Su, J., Zhang, X., Hu, N., Fu, G., Zhang, H., 2004. Geochemical characteristics and genesis of adakite-like granites at Yema Nanshan in the western segment of the Central Qilian Mountains. Chinese Geology (In Chinese with English abstract) 31 (4), 365–371. https://doi.org/10.1016/j.geothermics.2014.04.002.
- Su, Q., Yuan, D., Zhang, H., Manopkawee, P., Zhan, Y., Zhang, P., Xie, H., 2019. Geomorphic evidence for northeastward expansion of the eastern Qilian Shan, northeastern Tibetan Plateau. J. Asian Earth Sci. 177 (15), 314–323. https://doi.org/ 10.1016/j.jseaes.2019.04.003.
- Sun, Z., Yang, Z., Pei, J., Ge, X., Wang, X., Yang, T., Li, W., Yuan, S., 2005.
 Magnetostratigraphy of Paleogene sediments from northern Qaidam Basin, China: implications for tectonic uplift and block rotation in northern Tibetan plateau. Earth Planetary Sciences Letters 237 (3–4), 635–646. https://doi.org/10.1016/j.epsl.2005.

- Tapponnier, P., Zhiqin, X., Roger, F., Meyer, B., Arnaud, N., Wittlinger, G., Jingsui, Y., 2001. Oblique stepwise rise and growth of the Tibet Plateau. Science 294 (5547), 1671–1677. https://doi.org/10.1126/science.105978.
- Taylor, M., Yin, A., 2009. Active structures of the Himalayan-Tibetan orogen and their relationships to earthquake distribution, contemporary strain field, and Cenozoic volcanism. Geosphere 5 (3), 199–214. https://doi.org/10.1130/GES00217.1.
- Tseng, C., Yang, H., Yang, H., Liu, D., Wu, C., Cheng, C., Chen, C., Ker, C., 2009. Continuity of the North Qilian and North Qinling orogenic belts, Central orogenic system of China: evidence from newly discovered Paleozoic adaktic rocks. Gondwana Res. 16 (2), 285–293. https://doi.org/10.1016/j.gr.2009.04.003.
- Vermeesch, P., 2009. RadialPlotter: a Java application for fission track, luminescence and other radial plots. Radiat. Meas. 44 (4), 409–410. https://doi.org/10.1016/j. radmeas.2009.05.003.
- Vermeesch, P., 2012. On the visualisation of detrital age distributions. Chem. Geol. 312, 190–194. https://doi.org/10.1016/j.chemgeo.2012.04.021.
- Vincent, S.J., Allen, M.B., 1999. Evolution of the Minle and Chaoshui Basins, China: Implications for Mesozoic strike-slip basin formation in Central Asia. Geol. Soc. Am. Bull. 111 (5), 725–742. https://doi.org/10.1130/0016-7606(1999) 111 < 0725:EOTMAC > 2.3.CO;2.
- Wagner, G., 1968. Fission track dating of apatites. Earth Planet. Sci. Lett. 4, 411-415.
- Wan, J., Ma, L., Zhou, Z., 1989. Approach on the method for restoration of original sedimentary boundaries of the Cretaceous deformed basin in Jiouxi area. Petroleum Geology and Experiment (In Chinese with English abstract) 3, 245–249. https://doi. org/10.11781/sysydz198903245.
- Wan, J., Zheng, W., Zheng, D., Wang, W., Wang, Z., 2010. Low closure temperature thermochronometry study on the Late Cenozoic tectonic active of northern Qilianshan and its implication for dynamics of Tibetan Plateau growth. Geochimica (in Chinese with English abstract) 39 (5), 439–446.
- Wan, J., Zheng, D., Zheng, W., Wang, W., 2011. Modeling thermal history during low temperature by K-feldspar MDD and fission track: example from Meso-Cenozoic tectonic evolution in Saishitengshan in the northern margin of Qaidam basin. Seismology and Geology (in Chinese with English abstract) 33 (2), 369–382. https:// doi.org/10.1007/s11589-011-0776-4.
- Wang, X., Wang, B., Qiu, Z., Xie, G., Xie, J., Downs, W., Qiu, Z., Deng, T., 2003. Danghe area (western Gansu, China) biostratigraphy and implications for depositional history and tectonics of northern Tibetan Plateau. Earth Planetary Sciences Letters 208 (3–4), 253–269. https://doi.org/10.1016/s0012-821x(03)00047-5.
- Wang, F., Lo, C.-H., Li, Q., Yeh, M.-W., Wan, J., Zheng, D., Wang, E., 2004. Onset timing of significant unroofing around Qaidam basin, northern Tibet, China: constraints from 40Ar/39Ar and FT thermochronology on granitoids. J. Asian Earth Sci. 24 (1), 59–69. https://doi.org/10.1016/j.jseaes.2003.07.004.
- Wang, C., Zhao, X., Liu, Z., Lippert, P.C., Graham, S.A., Coe, R.S., Yi, H., Zhu, L., Liu, S., Li, Y., 2008. Constraints on the early uplift history of the Tibetan Plateau. Proc. Natl. Acad. Sci. U. S. A. 105 (13), 4987–4992. https://doi.org/10.1073/pnas.0703595105.
- Wang, W., Zhang, P., Kirby, E., Wang, L., Zhang, G., Zheng, D., Chai, C., 2011. A revised chronology for Tertiary sedimentation in the Sikouzi basin: implications for the tectonic evolution of the northeastern corner of the Tibetan Plateau. Tectonophysics 505 (1–4), 100–114. https://doi.org/10.1016/j.tecto.2011.04.006.
- Wang, C., Dai, J., Zhao, X., Li, Y., Graham, S., He, D., Ran, B., Meng, J., 2014. Outward-growth of the Tibetan Plateau during the Cenozoic: a review. Tectonophysics 621, 1–43. https://doi.org/10.1016/j.tecto.2014.01.036.
- Wang, Y., Zheng, J., Zheng, Y., Liu, X., Sun, G., 2015. Paleocene-Early Eocene uplift of the Altyn Tagh Mountain: evidence from detrital zircon fission track analysis and seismic sections in the northwestern Qaidam basin. Journal of Geophysical Research-Solid Earth 120 (12), 8534–8550. https://doi.org/10.1002/2015JB011922.
- Wang, W., Zhang, P., Pang, J., Garzione, C., Zhang, H., Liu, C., Zheng, D., Zheng, W., Yu, J., 2016a. The Cenozoic growth of the Qilian Shan in the northeastern Tibetan Plateau: a sedimentary archive from the Jiuxi Basin. Journal of Geophysical Research-Solid Earth 121 (4), 2235–2257. https://doi.org/10.1002/2015JB012689.
- Wang, W., Zhang, P., Yu, J., Wang, Y., Zheng, D., Zheng, W., Zhang, H., Pang, J., 2016b. Constraints on mountain building in the northeastern Tibet: detrital zircon records from synorogenic deposits in the Yumen Basin. Sci. Rep. 6, 27604. https://doi.org/ 10.1038/crep.27604
- Wang, W., Zheng, W., Zhang, P., Li, Q., Kirby, E., Yuan, D., Zheng, D., Liu, C., Wang, Z., Zhang, H., Pang, J., 2017. Expansion of the Tibetan Plateau during the Neogene. Nat. Commun. 8, 15887. https://doi.org/10.1038/ncomms15887.
- Wang, W., Zheng, D., Li, C., Wang, Y., Zhang, Z., Pang, J., Wang, Y., Yu, J., Wang, Y., Zheng, W., Zhang, H., 2020. Cenozoic exhumation of the Qilian Shan in the north-eastern Tibetan Plateau: evidence from low-temperature thermochronology. Tectonics, e2019TC005705. https://doi.org/10.1029/2019TC005705.
- Wei, Y., Zhang, K.X., Ji, J.L., Song, B.W., Jiang, S.S., Ke, X., 2013. Cenozoic sedimentation rate evolution of Qaidam Basin in the Tibetan Plateau and its response to the uplift of the plateau. Geological Bulletin of China 32 (1), 105–110 (in Chinese with English abstract).
- Wu, C., Yao, S., Zeng, L., Yang, J., Wooden, J., Chen, S., Mazadab, F., 2006. Double subduction of the early Paleozoic North Qilian oceanic plate: evidence from granites in the central segment of North Qilian. NW China: Geology in China 33 (6), 1197–1208. https://doi.org/10.1111/j.1749-6632.1962.tb34654.x. (in Chinese with English abstract).
- Wu, C., Xu, X., Gao, Q., Li, X., Lei, M., Gao, Y., Frost, B.R., Wooden, J., 2010. Early Palaeozoic granitoid magmatism and tectonic evolution in North Qilian, NW China. Acta Petrologica Sinica (in Chinese with English abstract) 26 (4), 1027–1044.
- Wu, C., Yin, A., Zuza, A.V., Zhang, J., Liu, W., Ding, L., 2016. Pre-Cenozoic geologic history of the central and northern Tibetan Plateau and the role of Wilson cycles in constructing the Tethyan orogenic system. Lithosphere 8 (3), 254–292. https://doi. org/10.1130/L494.1.

Wu, C., Zuza, A.V., Yin, A., Liu, C., Reith, R.C., Zhang, J., Liu, W., Zhou, Z., 2017. Geochronology and geochemistry of Neoproterozoic granitoids in the central Qilian Shan of northern Tibet: reconstructing the amalgamation processes and tectonic history of Asia. Lithosphere 9 (4), 609–636. https://doi.org/10.1130/L640.1.

- Wu, C., Liu, C., Fan, S., Zuza, A.V., Ding, L., Liu, W., Ye, B., Yang, S., Zhou, Z., 2019a. Structural analysis and tectonic evolution of the western domain of the Eastern Kunlun Range, northwest Tibet. Geol. Soc. Am. Bull. https://doi.org/10.1130/ B35388 1
- Wu, C., Zuza, A.V., Zhou, Z., Yin, A., McRivette, M.V., Chen, X., Ding, L., Geng, J., 2019b. Mesozoic-Cenozoic evolution of the Eastern KunlunRange, central Tibet, and implications for basin evolution during the Indo-Asian collision. Lithosphere 11 (4), 524–550. https://doi.org/10.1016/S0040-1951(03)00053-2.
- Xia, X., Song, S., Niu, Y., 2012. Tholeiite-boninite terrane in the North Qilian suture zone: Implications for subduction initiation and back-arc basin development. Chem. Geol. 328 (18), 259–277. https://doi.org/10.1016/j.chemgeo.2011.12.001.
- Xiao, W., Windley, B.F., Yong, Y., Yan, Z., Yuan, C., Liu, C., Li, J., 2009. Early Paleozoic to Devonian multipleaccretionary model for the Qilian Shan. NW China J. Asian Earth Sci. 35 (3-4), 323-333. https://doi.org/10.1016/j.jseaes.2008.10.001.
- Xiong, Z., Zhang, H., Zhang, J., 2012. Petrogenesis and tectonic implications of the Maozangsi and Huangyanghe granitic intrusions in Lenglongling area, the eastern part of North Qilian Mountain, NW China. Earth Science Frontiers (In China with English abstract) 19 (3), 214–227.
- Yan, M., Fang, X., Van Der Voo, R., Song, C., Li, J., 2013. Neogene rotations in the Jiuquan Basin, Hexi Corridor, China. Geological Society London Special Publications 373 (1), 173–189. https://doi.org/10.1144/sp373.6.
- Yang, S., Chen, H., Cheng, X., Xiao, A., He, G., Chen, J., Tian, D., 2007. Deformation characteristics and rules of spatial change for the Northern Qilian Shan thrust belt. Earth Science Frontiers (In Chinese with English abstract) 14 (5), 211–221. https://doi.org/10.3321/j.issn:1005-2321.2007.05.021.
- Yin, A., 2006. Cenozoic tectonic evolution of the Himalayan orogen as constrained by along strike variation of structural geometry, exhumation history, and foreland sedimentation. Earth Sci. Rev. 76 (1–2), 1–131. https://doi.org/10.1016/j.earscirev. 2005.05.004.
- Yin, A., 2010. Cenozoic tectonic evolution of Asia: a preliminary synthesis.

 Tectonophysics 488 (1–4), 293–325, https://doi.org/10.1016/j.tecto.2009.06.002.
- Yin, A., Harrison, T., 2000. Geologic evolution of the Himalayan-Tibetan orogeny. Annu. Rev. Earth Planet. Sci. 28, 211–280. https://doi.org/10.1146/annurev.earth.28.1.
- Yin, A., Nie, S., 1996. A Phanerozoic palinspastic reconstruction of China and its neighboring regions. In: Yin, A., Harrison, T.M. (Eds.), The Tectonics of Asia. Cambridge University Press, New York, pp. 442–485.
- Yin, A., Rumelhart, P.E., Butler, R., Cowgill, E., Harrison, T.M., Foster, D.A., Ingersoll, R.V., Zhang, Q., Zhou, X., Wang, X., Hanson, A., Raza, A., 2002. Tectonic history of the Altyn Tagh fault system in northern Tibet inferred from Cenozoic sedimentation. Geol. Soc. Am. Bull. 114 (10), 1257–1295. https://doi.org/10.1130/0016-7606(2002)114 < 1257; thotat > 2.0.co; 2.
- Yin, A., Dang, Y., Zhang, M., McRivette, M., Burgess, W., Chen, X., 2007a. Cenozoic tectonic evolution of Qaidam Basin and its surrounding regions (part 2): wedge tectonics in southern Qaidam Basin and the Eastern Kunlun Range. In: Sears, J.W., Harms, T.A., Evenchick, C.A. (Eds.), Whence the Mountains? Inquiries Into the Evolution of Orogenic Systems: A Volume in Honor of Raymond A. Price: Geological Society of America Special Paper. 433. pp. 369–390. https://doi.org/10.1130/2007.2433 (18)
- Yin, A., Manning, C.E., Lovera, O., Menold, C.A., Chen, X., Gehrels, G.E., 2007b. Early Paleozoic tectonic and thermomechanical evolution of ultrahigh-pressure (UHP) metamorphic rocks in the northern Tibetan Plateau, northwest China. Int. Geol. Rev. 49 (8), 681–716. https://doi.org/10.2747/0020-6814.49.8.681.
- Yin, A., Dang, Y., Wang, L., Jiang, W., Zhou, S., Chen, X., Gehrels, G.E., McRivette, M.W.,
 2008a. Cenozoic tectonic evolution of Qaidam Basin and its surrounding regions (part
 1): the southern Qilian Shan–Nan Shan thrust belt and northern Qaidam Basin. Geol.
 Soc. Am. Bull. 120 (7–8), 813–846. https://doi.org/10.1130/B26180.1.
- Yin, A., Dang, Y., Zhang, M., Chen, X., McRivette, M.W., 2008b. Cenozoic tectonic evolution of the Qaidam Basin and its surrounding regions (part 3): structural geology, sedimentation, and regional tectonic reconstruction. Geol. Soc. Am. Bull. 120 (7–8), 847–876. https://doi.org/10.1130/B26232.1.
- Yu, X., Guo, Z., Zhang, Q., Cheng, X., Du, W., Wang, Z., Bian, Q., 2017. Denan Depression controlled by northeast-directed Olongbulak thrust zone in northeastern Qaidam Basin: implications for growth of northern Tibetan Plateau. Tectonophysics 717, 116–126. https://doi.org/10.1016/j.tecto.2017.06.017.
- Yu, J., Pang, J., Wang, Y., Zheng, D., Liu, C., Wang, W., Li, Y., Li, C., Xiao, L., 2019. Mid-Miocene uplift of the northern Qilian Shan as a result of the northward growth of the northern Tibetan Plateau. Geosphere 15 (2), 1–10. https://doi.org/10.1130/GES01520.1.
- Yuan, W.M., Zhang, X.T., Dong, J.Q., Tang, Y.H., Yu, F.S., Wang, S.C., 2003. A new vision of the intracontinental evolution of the eastern Kunlun Mountains, Northern Qinghai-

- Tibet plateau, China. Radiat. Meas. 36 (1–6), 357–362. https://doi.org/10.1016/S1350-4487(03)00151-3.
- Yuan, W., Dong, J., Carter, A., Bao, Z., An, Y., 2006. Mesozoic-Tertiary exhumation history of the Altai Mountains, northern Xinjiang, China: constraints from apatite fission track data. Tectonophysics 412 (3–4), 183–193. https://doi.org/10.1016/ji tecto.2005.00.007
- Yuan, D., Ge, W., Chen, Z., Li, C., Wang, Z., Zhang, H., Zhang, P., Zheng, D., Zheng, W., Craddock, W.H., Dayem, K.E., Duvall, A.R., Hough, B.G., Lease, R.O., Champagnac, J.D., Burbank, D.W., Clark, M.K., Farley, K.A., Garzione, C.N., Kirby, E., Molnar, P., Roe, G.H., 2013. The growth of northeastern Tibet and its relevance to large-scale continental geodynamics: a review of recent studies. Tectonics 32 (5), 1358–1370. https://doi.org/10.1002/tect.20081.
- Zhang, H., Craddock, W.H., Lease, R.O., Wang, W., Yuan, D., Zhang, P., Molnar, P., Zheng, D., Zheng, W., 2012. Magnetostratigraphy of the Neogene Chaka basin and its implications for mountain building processes in the north-eastern Tibetan Plateau. Basin Res. 24 (1), 31–50. https://doi.org/10.1111/j.1365-2117.2011.00512.x.
- Zhang, H., Zhang, P., Zheng, D., Zheng, W., Chen, Z., Wang, W., 2014. Transforming the Miocene Altyn Tagh fault slip into shortening of the north-western Qilian Shan: insights from the drainage basin geometry. Terra Nova 26 (3), 216–221. https://doi. org/10.1111/ter.12089.
- Zhao, Z., Fang, X., Li, J., 2001. Late Cenozoic magnetic polarity stratigraphy in the Jiudong Basin, northern Qilian Mountain. Science in China Series D Earth Sciences 44 (S1), 243–250. https://doi.org/10.1007/BF02911993.
- Zheng, D., Zhang, P., Wan, J., Yuan, D., Li, C., Yin, G., Zhang, G., Wang, Z., Wei, M., Chen, J., 2006. Rapid exhumation at ~8 Ma on the Liupan Shan thrust fault from apatite fission-track thermochronology: implications for growth of the northeastern Tibetan Plateau margin. Earth Planet. Sci. Lett. 248 (1–2), 198–208. https://doi.org/10.1016/j.epsl.2006.05.023.
- Zheng, D., Clark, M.K., Zhang, P., Zheng, W., Farley, K.A., 2010. Erosion, fault initiation and topographic growth of the North Qilian Shan (northern Tibetan Plateau). Geosphere 6 (6), 937–941. https://doi.org/10.1130/GES00523.1.
- Zheng, D., Wang, W., Wan, J., Yuan, D., Liu, C., Zheng, W., Zhang, H., Pang, J., Zhang, P., 2017. Progressive northward growth of the northern Qilian Shan-Hexi Corridor (northeastern Tibet) during the Cenozoic. Lithosphere 9 (3), 408–416. https://doi:10. 1130/L587.1.
- Zhou, S., Wang, X., Wang, J., Xu, L., 2006. A preliminary study on timing of the oldest Pleistocene glaciation in QinghaieTibetan Plateau. Quaternary Internationa 154-155, 44–51. https://doi.org/10.1016/j.quaint.2006.02.002.
- Zhu, D.C., Wang, Q., Zhao, Z.D., Chung, S.L., Cawood, P.A., Niu, Y., Liu, S.A., Wu, F.Y., Mo, X.X., 2015. Magmatic record of India-Asia collision. Sci. Rep. 5, 14289.
- Zhuang, G., Hourigan, J.K., Ritts, B.D., Kent-Corson, M.L., 2011. Cenozoic multiple-phase tectonic evolution of the northern Tibetan Plateau: Constraints from sedimentary records from Qaidam Basin, Hexi Corridor, and Subei Basin, northwest China. Am. J. Sci. 311 (2), 116–152. https://doi.org/10.2475/02.2011.02.
- Zhuang, G., Brandon, M.T., Pagani, M., Krishnan, S., 2014. Leaf wax stable isotopes from Northern Tibetan Plateau: implications for uplift and climate since 15 Ma. Earth and Planetary Sciences. Letters 390, 186–198. https://doi.org/10.1016/j.epsl.2014.01.
- Zhuang, G., Johnstone, S.A., Hourigan, J.K., Ritts, B.D., Robinson, A., Sobel, E.R., 2018. Understanding the geologic evolution of northern Tibetan Plateau with multiple thermochronometers. Gondwana Res. 58, 195–210. https://doi.org/10.1016/j.gr. 2018.02.014.
- Zuza, A.V., Yin, A., 2016. Continental deformation accommodated by non-rigid passive bookshelf faulting: an example from the Cenozoic tectonic development of northern Tibet. Tectonophysics 677–678, 227–240. https://doi.org/10.1016/j.tecto.2016.04. 007.
- Zuza, A.V., Robin, R., An, Y., Dong, S., Liu, W., Zhang, Y., Wu, C., 2013. Structural and tectonic framework of the Qilian Shan-Nan Shan thrust belt, Northeastern Tibetan Plateau. Acta Geologica Sinica (English Edition) 87 (supp), 1–3. https://doi.org/10.1111/1755-6724.12148 1.
- Zuza, A.V., Cheng, X., Yin, A., 2016a. Testing models of Tibetan Plateau formation with Cenozoic shortening estimates across the Qilian Shan-Nan Shan thrust belt. Geosphere 12 (2), 501–532. https://doi.org/10.1130/GES01254.1.
- Zuza, A.V., Li, B., Tremblay, M.M., Chen, X., Shuster, D.L., Yin, A., 2016b. Cenozoic Development of the Northern Tibetan Plateau and the Onset of Thrust and Strike-slip Faulting: Constraints From Apatite and Zircon (U-Th)/He and Fission-track Thermochronometry: San Francisco, California, American Geophysical Union, Fall Meeting 2016, Abstract T11A-2586.
- Zuza, A.V., Wu, C., Reith, R.C., Yin, A., Li, J., Zhang, J., Zhang, Y., Wu, L., Liu, W., 2018. Tectonic evolution of the Qilian Shan: an early Paleozoic orogen reactivated in the Cenozoic. Geol. Soc. Am. Bull. 130 (5–6), 881–925. https://doi.org/10.1130/ B31721.1.
- Zuza, A.V., Wu, C., Wang, Z., Levy, D.A., Li, B., Xiong, X., 2019. Underthrusting and duplexing beneath the northern Tibetan Plateau and the evolution of the Himalayan-Tibetan orogen. Lithosphere 11 (2), 209–231. https://doi.org/10.1130/L1042.1.